Chem Soc Rev

RSC Publishing

REVIEW ARTICLE

View Article Online
View Journal | View Issue

Cite this: *Chem. Soc. Rev.*, 2013, **42**, 1568

Metal coordination in photoluminescent sensing†

Zhipeng Liu,[ab] Weijiang He*[a] and Zijian Guo*[a]

Coordination chemistry plays an essential role in the design of photoluminescent probes for metal ions. Metal coordination to organic dyes induces distinct optical responses which signal the presence of metal species of interest. Luminescent lanthanide (Ln^{3+}) and transition metal complexes of d^6, d^8 and d^{10} configurations often exhibit unique luminescence properties different from organic dyes, such as high quantum yield, large Stokes shift, long emission wavelength and emission lifetimes, low sensitivity to microenvironments, and can be explored as lumophores to construct probes for metal ions, anions and neutral species. In this review, the design principles and coordination chemistry of metal probes based on mechanisms of PeT, PCT, ESIPT, FRET, and excimer formation will be discussed in detail. Particular attention will be given to rationales for the design of turn-on and ratiometric probes. Moreover, phosphorescent probe design based on Ln^{3+} and d^6, d^8 and d^{10}-metal complexes are also presented *via* discussing certain factors affecting the phosphorescence of these metal complexes. A survey of the latest progress in photoluminescent probes for identification of essential metal cations in the human body or toxic metal cations in the environment will be presented focusing on their design rationales and sensing behaviors. Metal complex-based photoluminescent probes for biorelated anions such as PPi, and neutral biomolecules ATP, NO, and H_2S will be discussed also in the context of their metal coordination-related sensing behaviors and design approaches.

Received 31st August 2012

DOI: 10.1039/c2cs35363f

www.rsc.org/csr

1. Introduction

Photoluminescence techniques are considered to be one of the most effective tools for the detection of a variety of analytes due to their high sensitivity and selectivity, and high temporal and spatial resolution.[1] The fine instrument manipulability, commercial availability, lower detection limit, and *in situ* and *in vivo*

[a] *State Key Laboratory of Coordination Chemistry, School of Chemistry and Chemical Engineering, Nanjing University, Nanjing 210093, P. R. China. E-mail: heweij69@nju.edu.cn, zguo@nju.edu.cn*

[b] *School of Chemistry and Chemical Engineering, Liaocheng University, Liaocheng, 252059, P. R. China*

† Part of the centenary issue to celebrate the Nobel Prize in Chemistry awarded to Alfred Werner.

Zhipeng Liu

Zhipeng Liu was born in Linyi, China in 1982. He received his PhD in chemistry from Nanjing University in 2010 under the supervision of Professor Dr Zijian Guo. He then joined the faculty of Liaocheng University in 2010. His research interests include (I) design and synthesis of new functional dyes; (II) small molecular fluorescent sensors for biorelated species.

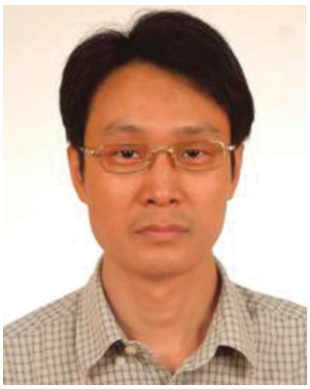

Weijiang He

Weijiang He was born in Jiangsu, China in 1969. He received his PhD degree in chemistry from Nanjing University in 2001. After a one year stay as a postdoc in the Max-Planck Institute of Colloids and Interfaces at Potsdam, he joined the State Key Laboratory of Coordination Chemistry, Nanjing University in 2003 and was promoted to full professor in 2009. His research interests include the fluorescent sensing and imaging of bioinorganic species, fluorescent investigation of artificial metalloenzymes, and photoactivable agents.

detection ability make the techniques extremely attractive in biological and environmental sciences.[1–6] Photoluminescent sensing and imaging of chemical species with biological and environmental significance has emerged as an important and fast developing field which is largely stimulated by improvement of confocal microscopy and optical imaging techniques. In the past decade, a great number of photoluminescent probes with various characteristics were reported. They could be applied for detection or imaging of specific molecules, microenvironments, biological processes and events. Several excellent books and reviews focused on the design principles and the application of fluorescent probes have been published.[1–3,7–18]

Metal coordination-induced alteration in photophysical, electrophysical or biological properties are essential for the related applications in photoluminescent sensing and detection. Most fluorescent probes for metal ions were developed based on metal coordination-induced alteration in emission intensity, lifetime or wavelength of organic dyes. The fluorescent emission of the metal complex comes from the radiative relaxation of π–π* excited states of organic dyes. Photoluminescent probes based on Ln^{3+} and transition metal cations of d^6, d^8 and d^{10} configurations emit differently from organic dyes, in which the luminescent emission comes from the radiative relaxation of metal-centered (MC, *via* LMCT process) or MLCT excited states.[19–23]

2. Metal coordination effect on the fluorescence of organic fluorophores and related probe design

Integrating an organic fluorophore as a fluorescence signal reporter with a specific chelator (receptor) is a common approach to design fluorescence probes for metal ions. In this case, metal coordination to the receptor will alter the fluorescence intensity, lifetime or excitation/emission maxima, reporting the presence of metal cations. The intramolecular interaction between the fluorophore and receptor is essential for the design of these fluorescent probes. Conventional mechanisms such as photo-induced electron transfer (PeT),[24,25] photo-induced charge transfer (PCT),[15] fluorescence resonance energy transfer (FRET)[26] and photo-induced excimer/exciplex formation have been frequently adopted for the construction of probe molecules.[27,28] On the other hand, a number of new rationales, such as metal ion coordination inhibited excited-state intramolecular proton transfer (ESIPT) and aggregation-induced emission (AIE), have also been explored to devise probes.[29]

2.1 Photo-induced electron transfer (PeT) and turn-on probes

PeT is the most widely employed mechanism for the design of fluorescence probes.[25] Classical PeT probes for metal cations contain three parts: fluorophore, spacer and ionophore (Fig. 1). Ionophores are normally electron donors (*e.g.* amino-containing group), while fluorophores are electron acceptors. For free probe, the electron occupying the highest occupied molecular orbital (HOMO) of the fluorophore can be promoted to the lowest unoccupied molecular orbital (LUMO) by absorbing an excitation photon. If the energy of the ionophore HOMO is just higher than that of the fluorophore, the electron of the ionophore HOMO will transfer to the HOMO of the excited fluorophore through space, which blocks the emission transition of the excited electron occupying the fluorophore LUMO to fluorophore HOMO. This fluorescence quenching effect is termed as photo-induced electron transfer (PeT). When the ionophore coordinates to the target metal ion, the energy gap between the two HOMO orbitals is changed from positive to negative due to the decreasing level of the ionophore HOMO *via* metal coordination, and the fluorescence of the probe is recovered. This metal chelation-enhanced fluorescence is also defined as metal chelation enhanced fluorescence (MCHEF) effect. In this case, the emission of the formed metal complex is ascribed mainly to the relaxation of the π–π* excited state of the organic fluorophore. Protonation of the ionophore may also lead to the blockage of the PeT process.

The PeT mechanism has been well discussed in the past thirty years and a large number of PeT probes for metal ions have been reported. However, PeT probes may suffer from certain shortcomings. For example, although the near-infrared (NIR) fluorescent probes are now more attractive than those of shorter excitation/emission wavelength due to their larger tissue penetration depth and lower phototoxicity, their higher fluorophore HOMO energy level decreases the energy gap between the HOMOs of the fluorophore and ionophore and reduces the efficiency of the PeT process to quench free probe emission.[30] Therefore, NIR probes with a PeT mechanism may suffer from high background fluorescence and lower analyte-induced emission enhancement factor. Therefore, the design of turn-on NIR probes with low background is still challenging. On the other hand, heavy metals ions like Hg^{2+} can quench fluorescence by several mechanisms,[31–35] and metal ions with un-paired electrons in their d-orbitals such as Cu^{2+} display a distinct ability to quench the emission of organic fluorophores

Zijian Guo

Zijian Guo was born in Hebei, China in 1961. After receiving his PhD degree from the University of Padua in 1994, he worked as a postdoc at the University of London, the University of British Columbia and the University of Edinburgh successively. He joined Nanjing University as a professor in 1999 and worked as the director of the State Key Laboratory of Coordination Chemistry from 2000 to 2009. He is currently the Chang Kang professor and dean of the School of Chemistry and Chemical Engineering, Nanjing University. His research interests include metal-based anticancer complexes, fluorescent sensors for biorelated metal cations, and metal-based artificial nucleases and proteases.

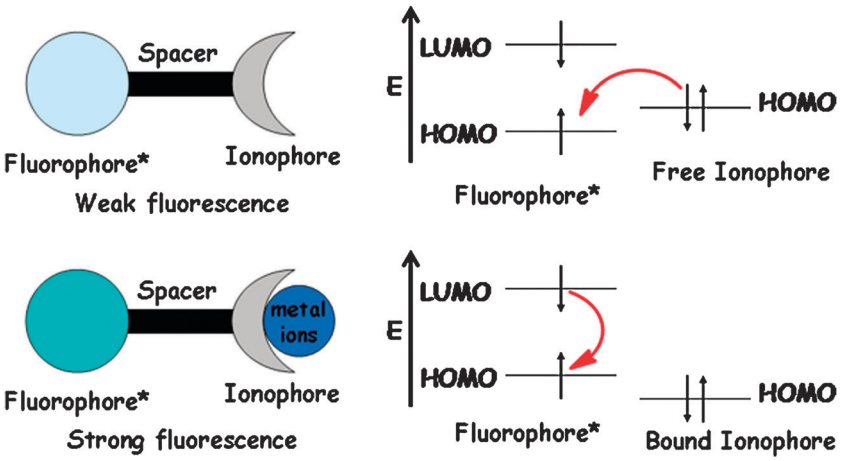

Fig. 1 PeT fluorescent probes for metal cations and their ''turn-on'' sensing mechanism.

via their un-paired electrons.[36] Therefore, the elaborative tuning of metal coordination *via* altering the ionophore and spacer structures to decrease both the metal paramagnetic nature and the spin–orbit coupling is essential for the design of turn-on PeT probes. In addition, two-photon excitable probes with a PeT mechanism for practical bioimaging applications are also currently attracting the interest of scientists.

2.2 Photo-induced charge transfer (PCT) and ratiometric probes

Internal charge transfer (ICT) fluorophores with a conjugated couple of electron-donating/electron-withdrawing groups (donor/acceptor, **D**/**A**), normally display large Stokes shift, visible light excitability and metal coordination-induced emission shift. Moreover, the ICT effect can decrease the basicity of the donor amine, which offers the opportunity to form probes with pH-independence in near-neutral pH conditions for application in biological systems. Modification of **D** or **A** as a metal ionophore results in metal coordination-induced blue or red shift of excitation/emission *via* altering the photo-induced internal charge transfer excited state, which provides an effective strategy to devise ratiometric metal ion probes. As shown in Fig. 2, metal coordination to the donor of an ICT fluorophore will decrease the HOMO energy and induce the hypsochromic

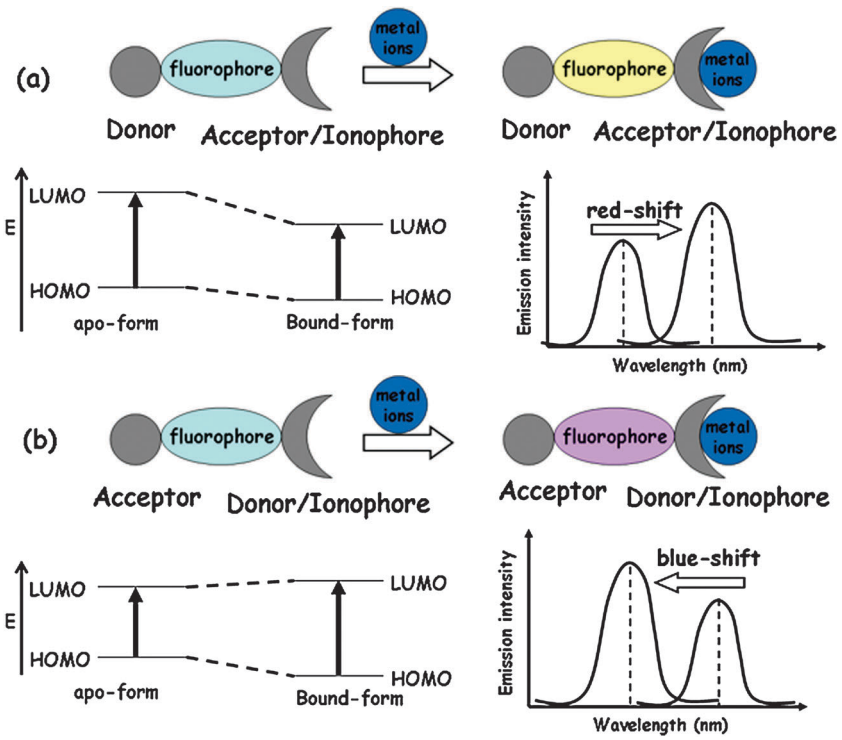

Fig. 2 PCT fluorescent probes for metal cations and their ratiometric sensing mechanisms.

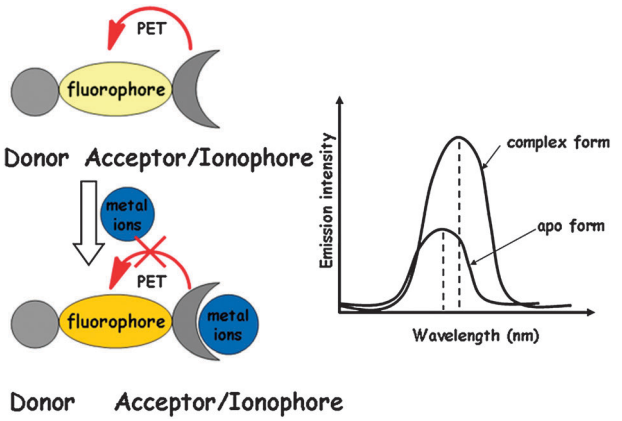

Fig. 3 Competition of PeT and PCT effects in fluorescent probes for metal cations.

shift of excitation or emission maxima. If there is metal coordination to its acceptor, the reverse change will be observed. These sensing behaviors are desirable for ratiometric probes, whose self-calibration effect of two excitation/emission bands can eliminate the interference of photobleaching and deviated microenvironments, local probe concentration and experimental parameters. Therefore, these probes allow quantitative determination of target metal ions in living cells, tissues and animals (Fig. 2).[37,38] Therefore, the PCT mechanism is an efficient strategy for the construction of ratiometric metal ion probes.[39]

Many probes designed following this approach, however, did not work or function as PCT probes, since the donor/acceptor modification may integrate electron donating atoms such as N or O into the ionophore, and the MCHEF effect will compete with the PCT response in the sensing system.[40,41] If the PeT process is dominant, the minor excitation/emission shift induced by metal coordination would be covered by the emission enhancement, and the probe functions as a PeT probe. If the metal coordination induced PCT process is more distinct and the alteration in intensity is minor, the probes are ratiometric ones (Fig. 3).[42] On the other hand, the PCT effect from donor to acceptor may decrease the metal coordination ability of the donor-derived ionophore, resulting in the photodisruption of metal coordination in the excited state and the absence of emission/excitation shift.[24,40] Therefore, the design of ratiometric probes based on the PCT effect is complicated and challenging.

2.3 Fluorescence resonance energy transfer (FRET) and ratiometric probes

Fluorescence resonance energy transfer, also known as Förster resonance energy transfer (FRET), is a non-radiative process in which the resonance energy transfers from an excited state of a donor fluorophore (**D-F**) to the ground state of an acceptor fluorophore (**A-F**) *via* a non-radiative "dipole–dipole coupling".[43] The emission spectrum of **D-F** should have a certain overlap with the absorption spectrum of **A-F**, and higher overlap will lead to more effective FRET. Moreover, FRET processes are distance-dependant, and a distance between **D-F** and **A-F** from 10 to 100 Å is required for an effective FRET (Fig. 4).[1,43]

The FRET mechanism is commonly exploited for the design of ratiometric fluorescent probes with large pseudo Stokes shifts. Three classes of FRET based metal ion probes have been frequently reported. The first is developed by linking a non-emissive moiety such as rhodamine spirolactam derivatives to a donating fluorophore. FRET can be switched on by binding of a metal ion to convert the non-emissive acceptor into a fluorophore (Fig. 5a). For instance, compound **1** (Fig. 6) is a ratiometric fluorescent Cr^{3+} probe based on FRET, in which 1,8-naphthalimide and rhodamine derivatives were selected as the **D-F** and **A-F**, respectively. There is no energy transfer between the two because of the non-emissive nature of rhodamine spirolactam derivatives. An efficient ring-opening reaction induced by Cr^{3+} generates fluorescent rhodamine, which induces an effective FRET process from naphthalimide to the switch-on rhodamine.[44] In this case, the probe normally functions as an emission ratiometric probe. If the metal-induced switch on is devised for **D-F**, then the probe is normally an excitation ratiometric one. It is clear the sensing selectivity comes from the selective response of the fluorophore precursor.

Tuning the overlap between the **D-F** emission spectrum and **A-F** absorption spectrum *via* metal coordination could also lead to a ratiometric response to metal cations. The ionophore of these types of probes is often conjugated directly with **D-F** or **A-F** (Fig. 5b). In this case, metal coordination to the ionophore would alter absorption/emission spectra of **D-F** or **A-F**. An exact example following this design rationale is probe **2** (Fig. 6), which is composed by integrating 5-(4-methoxystyryl)-5′-methyl-2,2′-bipyridine (bpy) with diamino-substituted naphthalimide (NDI) as **D-F** and **A-F**, respectively. It displays a specific Zn^{2+}-induced fluorescence enhancement *via* FRET. It was proposed that there was very small overlap between the emission spectrum of **D-F** and the absorption spectrum of **A-F** in the apo form,

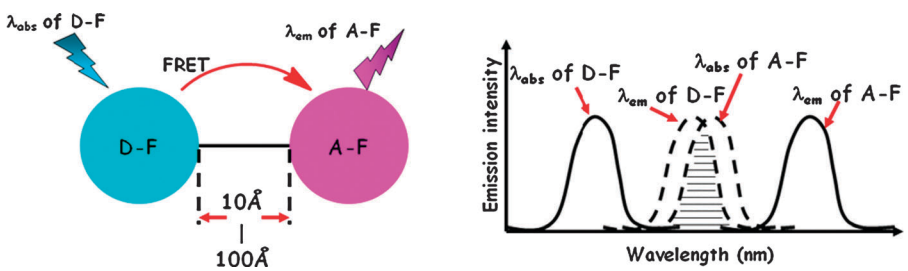

Fig. 4 Schematic diagram of the FRET process.

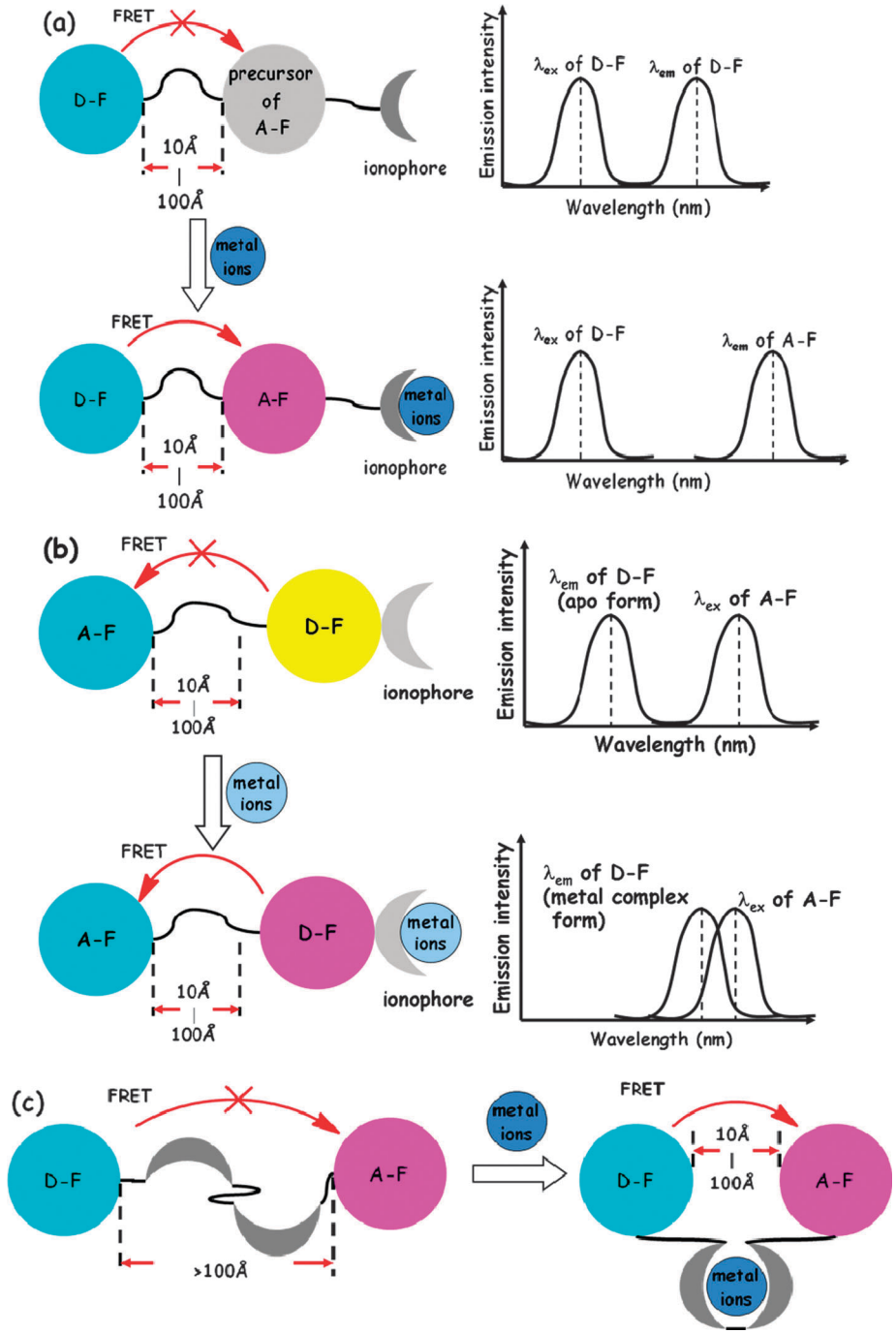

Fig. 5 Design principles of FRET-based fluorescent probes.

and Zn^{2+} coordination makes its emission band undergo a redshift which enables a significant spectral overlap between the emission of the bpy/Zn^{2+} complex and the absorption band of NDI. This facilitates the occurrence of FRET.[45] Although the author only reported the emission enhancement, a ratiometric response can be expected. The colorimetric or fluorescent response of the donor or acceptor fluorophore to certain metal cations determines the selective ratiometric response of these FRET probes.

The third class of FRET probes for metal ions functions mainly by tuning the dipole–dipole distance between **D-F** and **A-F** *via* metal coordination. For these probes, a spacer acting as an ionophore was demanded. In the apo form, the distance between **D-F** and **A-F** is longer than 100 Å, and FRET is switched off. Upon metal addition, the metal coordination of the spacer will alter the spacer conformation, resulting in the reduced distance between **D-F** and **A-F** and favoring the FRET process (Fig. 5c). To date, most of the probes of this type are protein-based.[46,47] For example, He and co-workers reported an Amt1-based Cu^{+} fluorescent probe, Amt1-FRET (**3**, Fig. 6), which consists of a Cu^{+}-binding domain of Amt1 (residues 36–110)

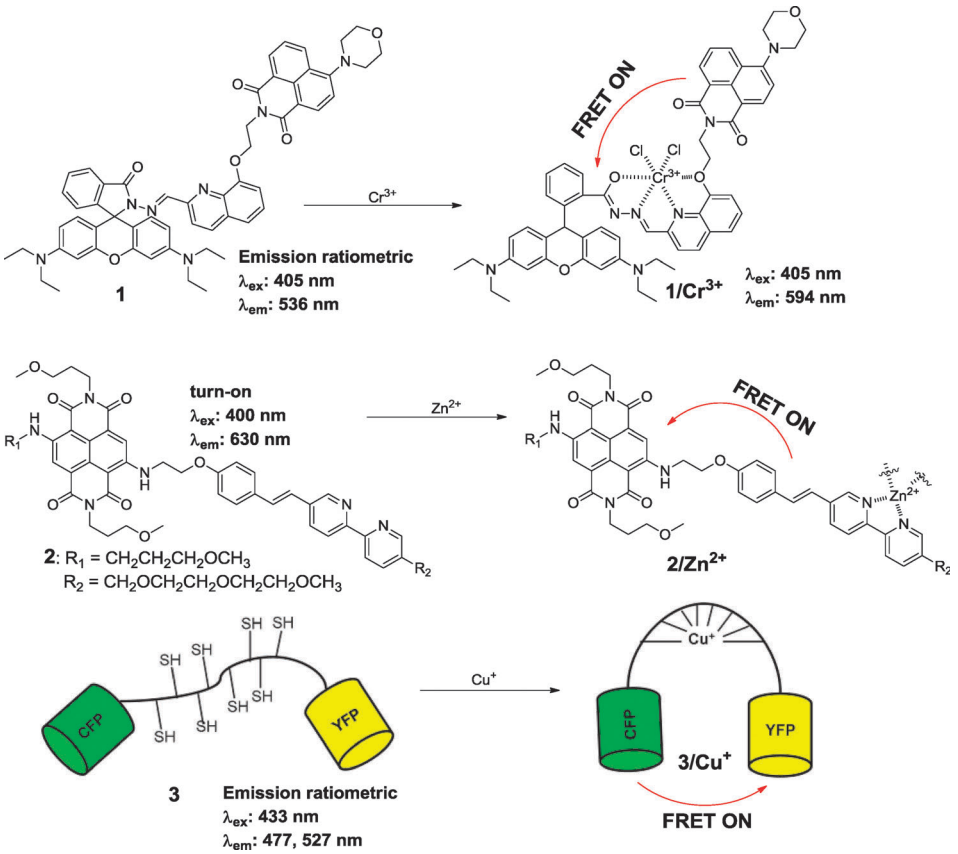

Fig. 6 Fluorescent probes **1–3** based on a FRET mechanism.

between a cyan fluorescent protein (CFP) and a yellow fluorescent protein (YFP). The coordination of Cu^{+} with Amt1 changed the conformation of Amt1 and resulted in effective FRET from CFP to YFP.[48] In this case, the selectivity of the spacer ionophore to metal cations determines the probe selectivity, and elaborative design of this ionophore spacer is essential.

2.4 Excimer formation and ratiometric probes

An excimer is formed by a fluorophore in the excited state with another fluorophore molecule in the ground state *via* weak interactions (*e.g.* π–π* stacking).[8] A typical metal ion probe functioning *via* excimer formation consists of two identical fluorophore moieties spaced by a flexible spacer which is also an ionophore. After coordinating with metal ions, the altered spacer makes the two fluorophore moieties become close (within van der Waals contact) which results in effective weak interactions between the two fluorophores. In this way, electronic excitation of one fluorophore causes an enhanced interaction with its neighbour, leading to the formation of an excimer. Compared to the monomer, the excimer typically provides a red-shifted and broad emission band. In most cases, both emission bands of the monomer and excimer can be observed simultaneously. Therefore, the metal coordination to the spacer ionophore can effectively alter the ratio between monomer emission and excimer emission, and excimer formation becomes an approach to ratiometric probes for metal cations (Fig. 7). Several probes based on this mechanism have been reported by Kim's group for the detection of Cu^{2+}.[49,50]

These probes generally require highly π-delocalized planar systems such as pyrene as the monomer. Therefore, they normally display poor aqueous solubility. Moreover, the excimer formation is highly dependent on the distance resulting from metal coordination, which is difficult to predict. The two factors limit the practical application of this rationale to the design of ratiometric probes.

2.5 Excited-state intramolecular proton transfer (ESIPT) and ratiometric probes

Organic molecules exhibiting excited-state intramolecular proton transfer (ESIPT) are sensitive to the surrounding medium and demonstrate emission of a large Stokes shift.[51,52] The energy level of the excited state of these molecules tends to decrease *via* transferring a hydroxyl (or amino) proton to a neighboring hydrogen-bonding atom (*e.g.* carbonyl oxygen, or imine nitrogen) through a pre-existing six- or five-membered ring of hydrogen bonding configuration. The ESIPT is a very fast process and occurs in a subpicosecond time scale. The energetically favored enol-form (Form **I**) is recovered spontaneously by reversed proton transfer after the relaxation of the ketol-form (Form **II**) to the ground state. The ESIPT process yields a large Stokes shift of emission due to the formation of a more stable excited molecule, tautomer S_1'. If the acidity of the hydroxyl (or amino)

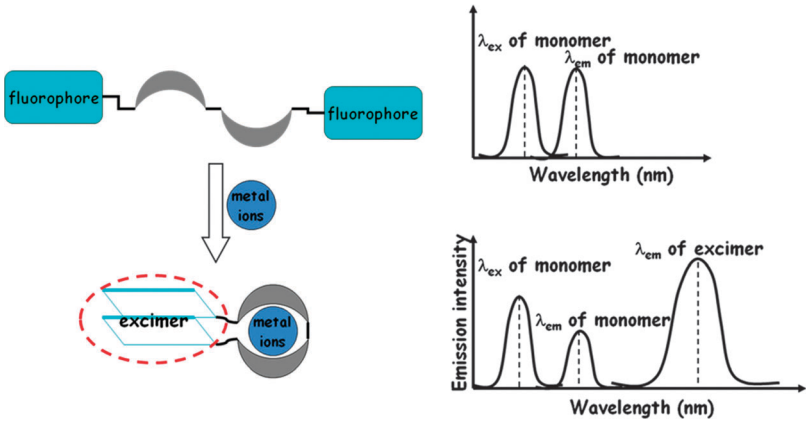

Fig. 7 Excimer formation-based fluorescent sensing.

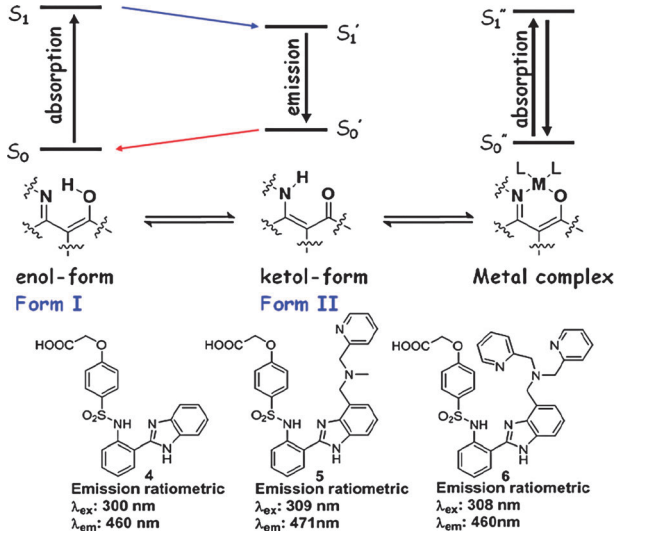

Fig. 8 Principle of ESIPT fluorescent probes for metal cations and emission ratiometric Zn^{2+} probes **4–6** based on this mechanism.

proton is sufficiently high, metal coordination will remove this proton and disrupt the ESIPT process, and a significant blue-shift in the emission is expected (Fig. 8). Fahrni and co-workers reported four benzimidazole derivatives (**4–6**) as ratiometric Zn^{2+} probes based on the ESIPT mechanism. These compounds show typical ESIPT induced emission at around 460–470 nm in PIPES solution (10 mM, pH 7.0, 0.1 M KCl). Upon Zn^{2+} coordination, the ESIPT processes were inhibited and blue-shifted emission (~50 nm) was observed. Therefore, metal coordination induced inhibition of ESIPT could be a promising approach for the development of ratiometric probes for metal ions.[51–53]

It should be noted that the overall fluorescence emission spectra of ESIPT fluorophores are often strongly influenced by pH, hydrogen bonding ability as well as polarity of the solvent. Moreover, the excitation wavelength of most reported ESIPT fluorophores is in the UV-vis range.[51–53] These features may hinder the practical use of these ESIPT probes in bioimaging.

2.6 Metal coordination induced chemical reactions and chemodosimeters

Most transition metal ions have electron withdrawing ability and act as Lewis acids, which can promote or catalyze certain chemical reactions. Therefore chemodosimeters for metal cations can be constructed based on a mechanism of metal-induced formation of an emissive fluorophore from a non-fluorescent precursor.[54] In fact, this approach is frequently used in the design of turn-on probes for metal cations with an emission quenching nature, such as Hg^{2+}, Cu^{2+}, and Fe^{3+}/Fe^{2+}. Most of these probes are based on metal induced-opening of the non-fluorescent spirolactam of xanthenes. The first example based on this reaction was reported in 1997 by Czarnik and co-workers, for a rhodamine B-based fluorescent probe for Cu^{2+} (Fig. 9).[55,56] Other metal coordination induced reactions, such as the hydrolysis of esters/hydrazides/ethers, rearrangement, and ring formation, have also been successfully employed for the development of other chemdosimeters.[54] If an additional donor or acceptor fluorophore is integrated in this system, then ratiometric probes can also be obtained just as shown in Part 2.3 for FRET-based ratiometric probes. Although many

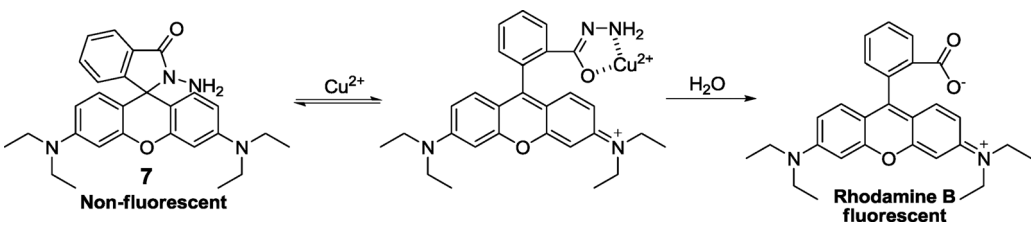

Fig. 9 Cu^{2+}-coordination-induced hydrolysis of rhodamine B hydrazide **7**.

metal chemodosimeters have been reported,[54,56] these probes often show slow and irreversible responses, disfavoring their application in tracking metal cations in living systems.

3. Metal coordination induced phosphorescence for sensing and imaging

Emissive metal complexes often feature a high quantum yield, large Stokes shift, long emission wavelength and lifetimes, and fine water solubility. Their emission is often pH-independent with low sensitivity to the microenvironment, which offers additional advantages over organic fluorophores. These metal complexes are potential fluorescent reporters for the design of photoluminescent probes. The most interesting examples reported so far are based on luminescent lanthanide complexes (Ln^{3+} complex, Ln^{3+} = Sm, Eu, Tb, Dy, Yb),[19,20,57] or transition metal complexes with d^6, d^8 and d^{10} configurations (Ru^{2+}, Ir^{3+}, and Pt^{2+}).[21,22,58] According to their mechanism involved with the intersystem crossing (ISC), their emission is normally termed as phosphorescence.

3.1 Lanthanide complexes

The phosphorescence of lanthanide complexes (Ln^{3+} = Sm^{3+}, Eu^{3+}, Tb^{3+}, Dy^{3+}, Yb^{3+}) comes from the excitation-induced f–f transition, and complexes with lanthanide centers of f^0 and f^{14} configuration are non-luminescent. For half f-filled Ln^{3+}, their electron configuration will lead to a large energy gap between its ground and excited states, which makes it difficult for them to demonstrate luminescence within the visible light window. Since f–f transitions of Ln^{3+} ions are Laporte-forbidden, the low molar extinction coefficients are not sufficient for the direct excitation of these metal centers. This problem can be resolved by incorporating an antenna (in some cases, it also acts as a co-ligand) into the Ln^{3+} complex. After the antenna is excited from the ground state to its singlet excited state, it undergoes ISC to a triplet state. Then, the intramolecular energy transfer from the triplet state of the antenna to the excited state of Ln^{3+} occurs, followed by the luminescent f–f transition to the ground state of Ln^{3+}, which emits in the visible range.[59] Due to this luminescence mechanism, the emission lifetimes of the Ln^{3+} complexes are in the range of milliseconds and microseconds, and the emission phenomenon is also termed as phosphorescence or luminescence.

Compared with the short emission lifetime of most organic dyes (on the scale of nanoseconds), the long emission lifetimes of Ln^{3+} ions are favorable for minimizing interference from light scattering or autofluorescence *via* time-gated detection of an analyte in complex microenvironments such as cells, tissues or living animals.[60,61] The emission spectra of Ln^{3+} complexes are normally well separated. For example, the main $^7F_5 \rightarrow {}^5D_4$ and $^7F_4 \rightarrow {}^5D_4$ emission peaks of Tb^{3+} do not overlap with any emission peaks of Eu^{3+}. Moreover, the inner-shell orbitals of Ln^{3+} are scarcely affected by other factors, therefore, the emission bands of Ln^{3+} complexes are normally narrow ($\sim$20 nm), which offers these complexes additional advantages in multicolor imaging.[23] The large Stokes shift from the antenna absorption to Ln^{3+} emission and the tunable quantum yield are additional attractive optical properties of Ln^{3+} complexes, which make them a suitable platform for the design of luminescent probes. Luminescent complexes of Eu^{3+} and Tb^{3+} are the most employed due to the low sensitivity of their excited states to vibrational quenching effects caused by energy transfer to OH, NH, or CH oscillators, which occur frequently in solution and imaging microenvironments.

The quantum yield of Ln^{3+} complexes has been associated with several major factors.[23,57] The energy level of the antenna triplet state should be at least 1700 cm^{-1} above the excited states of Ln^{3+}, and too high or too low energy levels will lead to only the fluorescence of the antenna. If the energy level of the antenna triplet state is too close to the ^5D excited state of Ln^{3+}, back energy transfer from Ln^{3+} to the antenna will occur and consequently lead to the decrease of Ln^{3+} luminescence. On the other hand, the distance between the antenna and Ln^{3+} center should be favorable to realize the energy transfer from the antenna to Ln^{3+}. In addition, the coordination environment of the Ln^{3+} center is also closely associated with their luminescence efficiency and lifetime. Since Ln^{3+} centers prefer high coordination numbers ($\geqslant$6) and display high affinity to hard ligands, many Ln^{3+} complexes undergo ligand exchange with solvents such as water, which triggers non-emissive scattering processes and reduces significantly the quantum yield. Therefore, elaborative design of both antenna ligand and other co-ligands is important to achieve Ln^{3+}-based luminescent probes for specific analytes.

Three classes of luminescent Ln^{3+} complex-based probes are shown in Fig. 10. In the first class, the probes function *via* analyte-induced formation or alteration of the antenna. For metal cation probes, a chromophore or chromophore precursor is integrated into the Ln^{3+} complex as an ionophore, which will change its triplet state energy level or form a new chromophore to alter the energy transfer from the antenna triplet state to the Ln^{3+} center upon coordinating to the targeted metal cation (Fig. 10a). This design rationale can be clearly demonstrated with the Eu^{3+} complex-based Zn^{2+} probes reported by Nagano and co-workers, which will be discussed in Part 4.2.3.[62]

In the second class of Ln^{3+} complex-based probes, the distance between the antenna and Ln^{3+} center is altered by the analyte. The distance change can be achieved by different approaches. If an ionophore is introduced to bridge the antenna and Ln^{3+} complex moiety, the targeted metal cation coordination to the ionophore will reduce the distance between the antenna and Ln^{3+} and promote the energy transfer from the antenna triplet state to the Ln^{3+} center, which triggers phosphorescence enhancement and reports the presence of the targeted metal cation (Fig. 10b). This approach has been adopted by Pierre and co-workers to devise probe **8** (**Tb-1**, Fig. 11) for the time-gated luminescence sensing of K^+.[63] In probe **8**, the terbium complex moiety was combined with its antenna, 5*H*-chromeno[2,3-*b*]pyridin-5-one, *via* an azacrown ether linker. The antenna is far away from Tb^{3+} in its apo form, which makes probe **8** display weak luminescence. Upon K^+ addition,

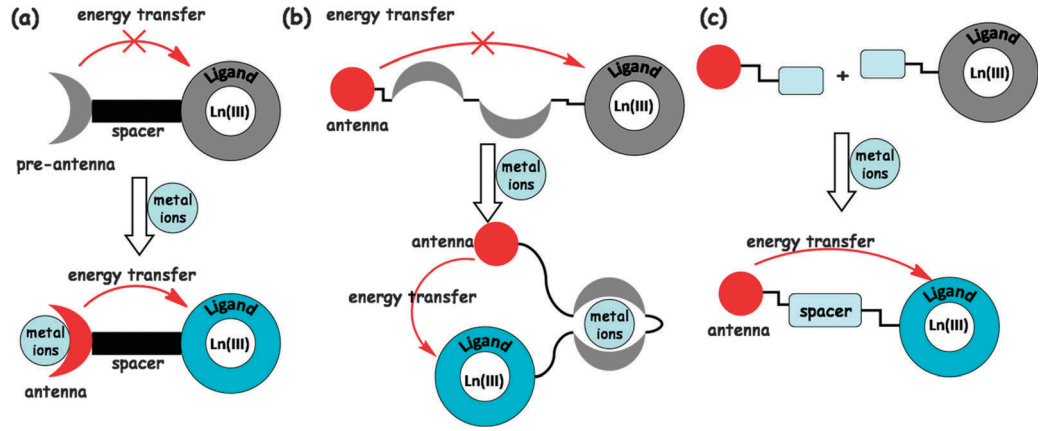

Fig. 10 Approaches to modulating the phosphorescence of Ln^{3+} complex-based probes *via* metal coordination-induced antenna formation or distance alteration.

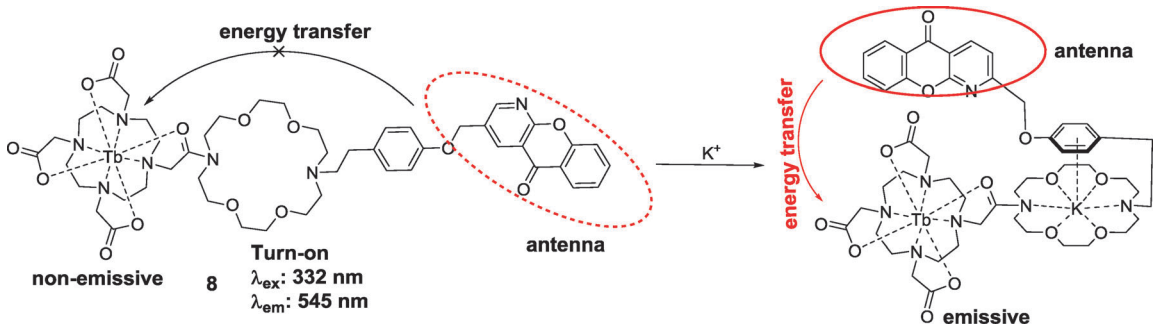

Fig. 11 Sensing mechanism of probe **8**.

the synergic K^+ binding *via* azacrown ether coordination and π–cation interaction reduce the distance between the Tb^{3+} center and antenna and facilitate the energy transfer from the antenna to the Tb^{3+} center. As a result, a specific K^+-induced luminescence enhancement can be achieved. Another frequently reported approach is based on the totally separated antenna chromophore and Ln^{3+} complex. Both are tagged with reactive sites or chelators for targeting metal ions. The two separated moieties can be unified to form a new complex containing both antenna and Ln^{3+} center *via* a synergic metal chelation or metal-induced coupling reaction. As a result, enhanced luminescence will be observed due to the effective energy transfer from the antenna to Ln^{3+} in the newly formed Ln^{3+} complex (Fig. 10c).

The third class of Ln^{3+} complex-based probes were designed profiting from an analyte-induced change of coordination environment or ligand exchange in solution (Fig. 12). Because of the long lifetimes of the ^5D excited states of the Ln^{3+} complex, the emission would be quenched *via* non-radiative energy transfer to nearby O–H or N–H oscillators of lower energy. Therefore, O–H and N–H containing ligands such as water molecules are excellent quenchers of Ln^{3+} complex luminescence. Anions or natural species with strong coordination ability to Ln^{3+} ions can replace coordinated O–H and N–H containing ligands, then the emission of the Ln^{3+} complex would be recovered. Parker and co-workers have reported a

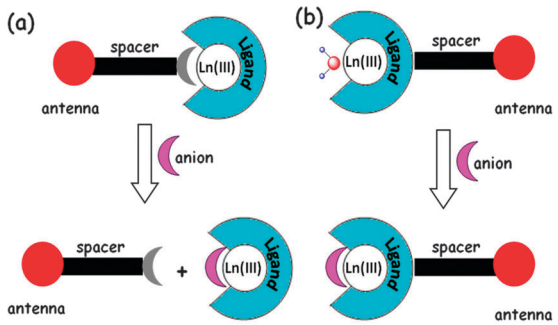

Fig. 12 Approaches to modulating the phosphorescence of Ln^{3+} complex-based probes *via* (a) displacement of a weakly coordinated antenna or (b) tuning the number of coordinated water molecules.

series of phosphorescent probes (**9**) for bicarbonate with this approach.[64,65] These complexes contain a single coordinated water molecule in the apo form, which can be readily displaced by the bicarbonate anion and display distinct luminescence enhancement. On the other hand, if the antenna functions as a co-ligand of the Ln^{3+} complex, its replacement *via* ligand exchange by targeting species will result in emission quenching. An Eu^{3+} complex probe (**10**) for HCO_3^- was developed with this strategy (Fig. 13). Displacement of antenna chromophore β-diketonate by chelating anion such as HCO_3^- decreases the luminescence of Eu^{3+}.[66]

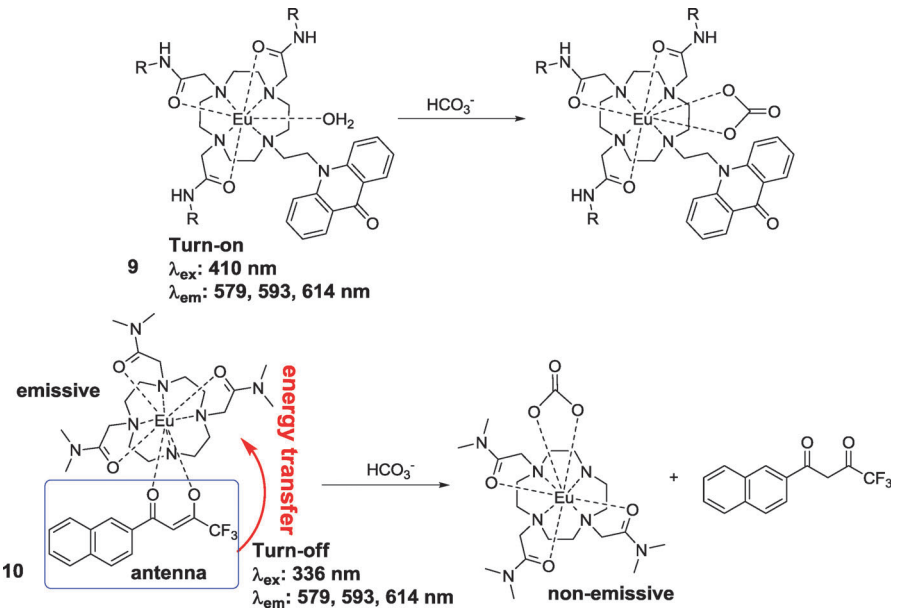

Fig. 13 Phosphorescent Ln^{3+} complex-based probes **9** and **10** functioning *via* tuning the number of coordinated water molecules or coordination displacement of antenna.

3.2 Transition metal complexes of d^6, d^8 and d^{10} configurations

Besides Ln^{3+} complexes, heavy-transition metal complexes of d^6, d^8 and d^{10} configuration with phosphorescence are another important class of chromophores for the construction of luminescent probes.[22] Similar to the f–f transitions, d–d transitions are also Laporte-forbidden. However, the strong spin–orbit coupling of these heavy transition metal complexes (normally second- and third-row transition metal complexes) can promote the ISC process from the singlet excited state to the triplet manifold, favoring the spin-forbidden T_1–S_0 radiative relaxation. The radiative relaxation to S_0 occurs at significantly slower time scales due to the spin-forbidden nature of $T_1 \rightarrow S_0$, resulting in phosphorescent emission with long radiative decay times.[67–69] In these transition metal complexes, those of d^6 and d^8 configuration (such as Re^I, Os^{II}, and Ir^{III}) display phosphorescence *via* a metal-to-ligand charge transfer (MLCT) in the excited state, while those of d^{10} configuration such as Cu^I, Ag^I, and Au^I emit normally *via* a ligand-to-metal charge transfer (LMCT) in the excited state.

These phosphorescent d-block transition metal complexes often show excellent photophysical properties such as large Stokes shifts, significant single-photon excitation in the visible range (λ_{ex} > 550 nm) and relatively longer lifetimes than organic fluorophores.[70–73] Their relatively long lifetime endows them a capacity for excellent temporal resolution, and their luminescence can be easily identified from fluorescent backgrounds. This merit provides phosphorescent d-block transition metal complex-based probes a possibility for lifetime-based imaging using fluorescence lifetime imaging microscopy (FLIM).[74] The design approaches for d-block transition metal complex-based phosphorescent probes are given in the following examples:

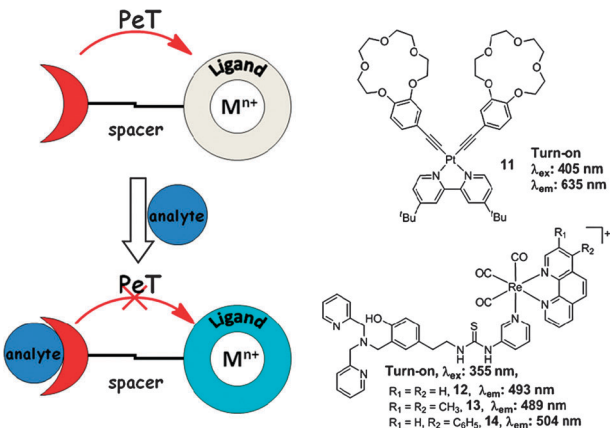

Fig. 14 PeT phosphorescent probes based on d-block transition metal complexes.

(1) The analyte receptor is combined with a phosphorescent d-block transition metal complex through a spacer (PeT-based phosphorescent probes, Fig. 14). In this case, the d-block transition metal complex is used just like an organic fluorophore. In the apo form, these PeT-based phosphorescent probes exhibit a quenched emission due to the PeT process from the receptor to the phosphor. After binding to the analyte, the PeT process is inhibited, which recovers the emission of the phosphor. Probes **11** and **12–14** shown in Fig. 14 are typical PeT probes based on the phosphorescent d-block transition metal complexes for the sensing of Zn^{2+}/Mg^{2+} and Zn^{2+}/Cd^{2+}.[75,76]

(2) The analyte receptor is directly linked to the chromophore ligand of the phosphorescent d-block transition metal complex (Fig. 15). Since the excited states of these emissive d-block transition metal complexes are complicated, which include MLCT,[77] LLCT (ligand-to-ligand charge transfer),[78,79]

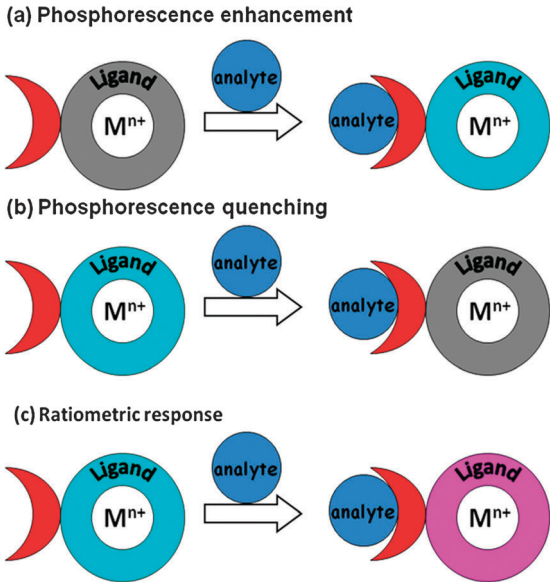

Fig. 15 Modulating the phosphorescence of d-block transition metal complex probes *via* conjugation of receptor to d-block transition metal complexes (a, b) or analyte-triggered chemical reaction (c).

LMCT,[80] ILCT (intraligand charge transfer),[81] MMLCT (metal–metal-to-ligand charge transfer),[82] LMMCT (ligand-to-metal–metal charge transfer)[83] and MLLCT (metal-to-ligand–ligand charge transfer)[84–86] states, the emission of these complexes is dependent on not only the metal centers but also the chemical structures and triplet state energy levels of its chromophore ligands. By conjugating a receptor into the ligand, the analyte binding would perturb the energy levels of the excited states, which results in a change of emission wavelength, quantum yield or lifetime. The Pt^{2+} terpyridyl complex (**15**) shown in Fig. 16 was reported as a colorimetric and phosphorescence turn-off probe for anion sensing.[87] Anions such as F^-, AcO^- and $H_2PO_4^-$ are able to quench the ^{3}MLCT dπ(Pt)–π^*(^{t}Bu$_3$terpyridine) emission *via* anion-induced deprotonation of the hydroxyl group. This emission quenching could be attributed to the deprotonation of the phenolic ethynyl ligand and enhancement

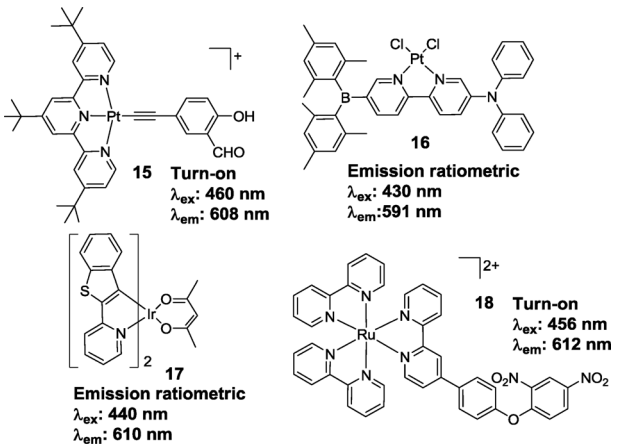

Fig. 16 Chemical structures of phosphorescent probes **15–18**.

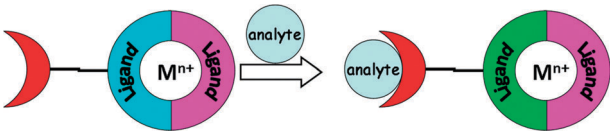

Fig. 17 Ratiometric sensing of analyte *via* heteroleptic d-block transition metal complex probes.

of charge transfer from the deprotonated phenolic ethynyl ligand to the excited state of the Pt^{2+} terpyridyl complex. As to **16**, a well-known F^- receptor $BMes_2$ was incorporated into the chromophore ligand of **16** as the electron acceptor (Fig. 16). **16** exhibits a phosphorescent ratiometric response to F^-, since the F^--triggered switching from ICT transition to π–π^* transition in the chromophore ligand alters the MLCT state effectively.[88] A sulfur atom is introduced into cyclometalated ligands in probe **17** as the Hg^{2+} binding site. Upon addition of Hg^{2+}, a sharp blue-shift of absorption and emission bands and positive shift of the Ir^{3+}/Ir^{2+} oxidation wave were observed. The coordination of sulfur to Hg^{2+} lowers the π electron density of the chromophore ligand and alters the MLCT state, resulting in the colorimetric and luminescent ratiometric sensing behavior of **17**.[89]

Phosphorescent chemodosimeters can be readily devised by integrating the reactive site into the ligand. For example, the Ru^{2+}-bipyridine complex derivative (**18**) shown in Fig. 16 was synthesized for thiophenol sensing.[90] The thiophenol-induced reaction triggers the cleavage of the electron acceptor group, 2,4-dinitrophenyl, and yields a new emissive phosphor, $[Ru(bpy)_2(HP\text{-}bpy)]^{2+}$. Moreover, **18** can be potentially used for imaging the dynamic intracellular process of thiophenol in living cells.

(3) Ratiometric phosphorescent probes based on heteroleptic d-block transition metal complexes (Fig. 17). When different ligands were introduced into an emissive d-block transition metal complex, various excited states such as MLCT, IL and ILCT could coexist in heteroleptic complexes. By tuning the electron donating/withdrawing ability of different ligands, dual emission bands could be observed (Fig. 17).[91–98] If an analyte binding site was integrated into a chromophore ligand, the metal coordination of the targeted metal cation will alter the MLCT state and lead to a ratiometric response.

4. Photoluminescent probes for metal cations and the metal coordination-related design rationales

Metal ions play vital roles in different biological systems. The design of related fluorescent probes are essential for their detection and tracking. Due to the limited scope of this article, we concentrate on summarizing newly reported fluorescent probes for bio-relevant metal ions including Zn^{2+}, Cu^+/Cu^{2+}, and Fe^{2+}/Fe^{2+} and toxic heavy-metal ions including Hg^{2+} and Cd^{2+} emphasizing the roles of metal coordination in the sensing process. The aforementioned metal coordination induced PeT,

PCT, FRET, ESIPT, excimer formation, *etc.* provide reliable design rationales for the construction of turn-on or ratiometric probes.

The major challenge in the design of fluorescent probes is how to discriminate different metal ions with similar chemical properties (*e.g.* Zn^{2+} and Cd^{2+}, Hg^{2+} and Ag^{+}). Hard and soft acids and bases theory (HSAB)[99] and Irving–Williams rule[100] are general guiding principles for the design of related metal ionophores. Coordination atom, coordination number, coordination geometry or cavity size are key factors to be modulated in designing an ionophore.[101,102] Additional non-covalent interactions may play synergetic roles in differentiating similar metal cations. For example, ancillary π–ligand and π–cation interactions favor the enhancement of the binding ability for soft transition metal cations from the second and third rows.

Among the essential transition metals in the human body, the top three most abundant elements are Fe (4–5 g), Zn (2–3 g) and Cu (~250 mg).[103] The disturbed homeostasis of iron, zinc and copper ions play causative roles in many diseases such as hepatitis, cancer, neurodegenerative Alzheimer's disease, Parkinson's disease, *etc.*[104–113] Considering the relative concentrations of Fe^{2+}/Fe^{3+}, Zn^{2+} and Cu^{+}/Cu^{2+} and the important roles they play in physiological/pathological processes, development of fluorescent probes for the biological sensing and imaging of these metal ions is of great significance.

4.1 Fluorescent probes for Fe^{3+}/Fe^{2+} and the related design rationales

Owing to the intrinsic paramagnetic quenching nature of Fe^{2+} and Fe^{3+},[114] fluorescent probes that exhibit a ''turn-on'' response towards Fe^{2+}or Fe^{3+} are rare. Since $Fe^{2+}$and Fe^{3+} can adopt variable coordination geometries such as octahedron, pyramidal, tetrahedron, and square planar,[115] it is difficult to construct an artificial ionophore with high selectivity for Fe^{2+} or Fe^{3+}, except for natural siderophores and artificial analogues. Therefore, most fluorescent probes for Fe^{3+} are based on small molecular siderophores.[116] The terpyridine moiety was also utilized in some studies, but its low binding selectivity is not very satisfactory. Two major challenges remain for the development of Fe^{2+} or Fe^{3+} fluorescent probes: ''turn-on'' and ratiometric sensing ability for Fe^{3+} or Fe^{2+}.

According to the approaches for turn-on probes discussed above, both PeT (Part 2.1) and chemodosimeter (Part 2.6) approaches are effective rationales for turn-on fluorescent probe. For the paramagnetic Fe^{3+}, the electron decoupling of Fe^{3+} from the fluorophore should favor to overcome the quenching effect of Fe^{3+} on the fluorophore and guarantee the turn-on response of a PeT probe for Fe^{3+}. Rurack and co-workers developed a new turn-on Fe^{3+} probe **19** by integrating a size-restricted dithia-aza-oxa macrocycle (DTAO), 1-oxa-4,10-dithia-7-aza-cyclododecane with a fluorophore *meso*-substituted boron-dipyrromethene (BDP) *via* a rigid phenyl linker. This probe displays mainly the ICT emission band at 634 nm and a minor local emission (LE) band at 508 nm in aqueous media. The distinct enhancement of the LE band upon Fe^{3+} addition displaying the PeT effect from DTAO to the BDP fluorophore has been blocked by Fe^{3+} coordination with ionophore DTAO. It seems that the electron decoupling of Fe^{3+} from the BDP fluorophore by the rigid spacer has isolated the BDP fluorophore from the emission quenching Fe^{3+} (Fig. 18). Moreover, Fe^{3+} induces the decrease of its ICT band in the meantime, therefore, this probe displays still a ratiometric sensing ability for Fe^{3+}.[117]

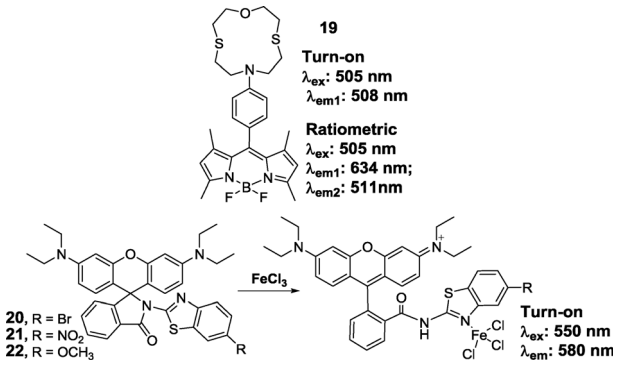

Fig. 18 Fe^{3+} turn-on probe **19** and Fe^{3+} sensing mechanism of turn-on chemodosimeters **20–22**.

The chemodosimeter approach based on the metal-induced conversion of a non-fluorescent compound to a fluorescent one (Part 2.6) is also a reliable means for the turn-on sensing of Fe^{3+} or Fe^{2+}. As reviewed recently by Yoon *et al.*,[56] a reversible equilibrium between the spirolactam and ring-opened forms of rhodamine triggered by Fe^{3+} can be an efficient approach to construct ''turn-on'' fluorescent Fe^{3+} probes. For example, by introducing different benzothiazole moieties into rhodamine, three rhodamine based ''turn-on'' fluorescent chemodosimeters (**20–22**) have been prepared (Fig. 18), which demonstrate high selectivity and sensitivity for Fe^{3+}.[118] These chemodosimeters show an Fe^{3+}-coordination induced ''turn-on'' fluorescence in water–methanol (5.5 : 4.5, v/v) solutions. The imaging application of three chemodosimeters for Fe^{3+} has been achieved in living HeLa cells. The crystal structure of the **22**/Fe^{3+} complex revealed that Fe^{3+} prefers to coordinate with the benzothiazole N atom rather than the carboxylic O atom, which was supported by DFT calculations.

For the ratiometric probe for Fe^{3+} or Fe^{2+}, the PCT and FRET approaches discussed in Parts 2.2 and 2.3 should be the dependent design rationales. For examples, based on the PCT approach, a ratiometric Fe^{3+} probe **23** was developed by linking a phenanthroimidazole derivative with a 2,2′-bipyridine motif.[119] Upon Fe^{3+} addition, **23** displays a ratiometric fluorescence response with the ratio of F_{440}/F_{500} being enhanced from 0.36 to 3.24 in aqueous solution (containing 50% methanol). The Fe^{3+} coordination to bipyridine to alter the ICT effect between the bipyridine and phenanthroimidazole motif is responsible for the ratiometric sensing behavior. Its detection limit for Fe^{3+} was estimated to be 5.26×10^{-6} M. The ratiometric probe for Fe^{3+} also has been devised based on the FRET approach shown in Fig. 5a. Therefore, a water-soluble supramolecular β-cyclodextrin–dye complex system formed by a dansyl-linked β-cyclodextrin and a spirolactam rhodamine-linked adamantane

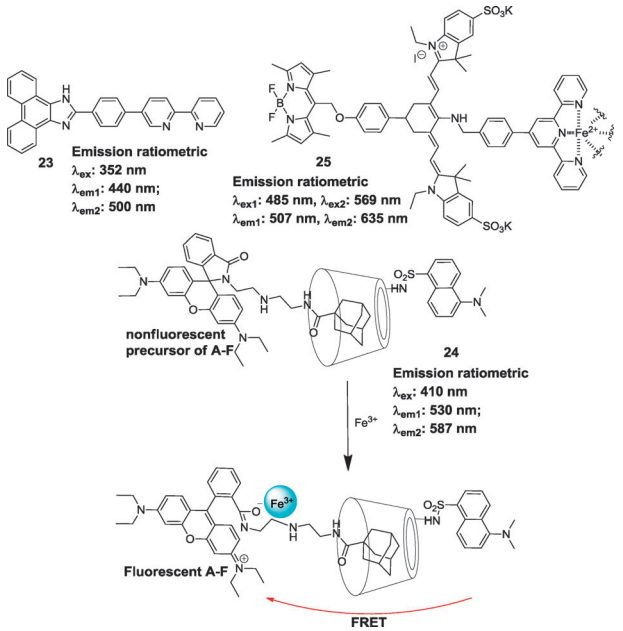

Fig. 19 Ratiometric probes **23–25** and the sensing mechanism of a supramolecular chemodosimeter for Fe^{3+}.

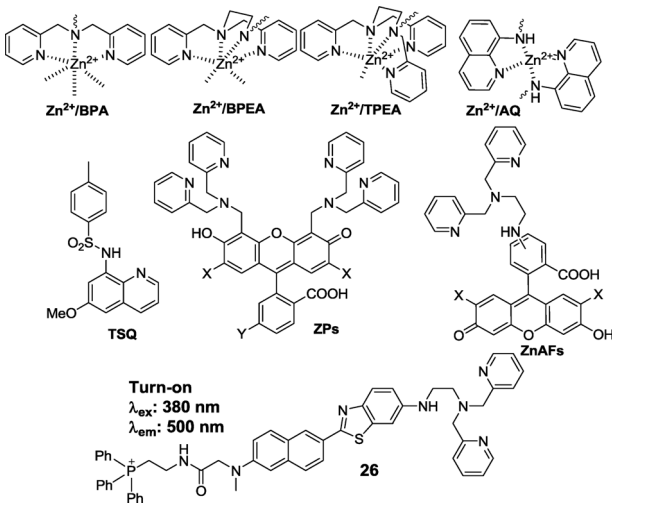

Fig. 20 Zn^{2+} coordination of BPA, BPEA, TPEA and AQ, and some examples of turn-on Zn^{+} fluorescent probes.

was developed as a FRET mechanism based ratiometric fluorescent chemodosimeter (**24**) for Fe^{3+}.[120] By anchoring the adamantyl moiety into the β-CD cavity, the supramolecular β-cyclodextrin–dye complex shows a sensitive and selective ratiometric response to Fe^{3+} in aqueous solution. Addition of Fe^{3+} into the solution of **24** results in a decrease in the emission band at 530 nm (dansyl) and an increase in the emission band at 587 nm (rhodamine). Fe^{3+}-induced spirolactam-opening makes the non-fluorescent rhodamine spirolactam convert into the fluorescent rhodamine as **A-F**, which triggers the effective FRET process from dansyl to rhodamine, displaying a ratiometric response to Fe^{3+} (Fig. 19).

A dual fluorophore hybridization approach which is not discussed in Parts 2 and 3 has also been successfully utilized to devise a ratiometric Fe^{2+} probe.[121] Therefore, a BDP derivative was linked to a cyanine dye to give a ratiometric probe **25**. Fe^{2+} binding to its 4′-phenyl-2,2′,6′,2″-terpyridine (Tpy) receptor quenched the emission of cyanine at 635 nm (F_{635}), while the emission of BDP at 507 nm (F_{507}) remains unchanged. In aqueous solution, **25** displays a selective ratiometric response to Fe^{2+} with a K_d of 2.5 μM. Moreover, **25** is capable of detecting the fluctuation of intracellular Fe^{2+} in HL-7702 cells. On the other hand, for the ICT fluorophore displaying both the LE and ICT emission bands, the different influence of Fe^{3+} on the two bands may also lead to the ratiometric sensing ability, it is exactly the same as in the case of probe **19** shown above.

4.2 Photoluminescent probes for Zn^{2+} and the related design rationales

The development of fluorescent probes for biological Zn^{2+} has been attracting considerable attention in recent years, since Zn^{2+} imaging *via* fluorescent probes offers spatiotemporal information which is essential for clarifying its homeostasis and physiological/pathological roles.[15,122–126] The most frequently used Zn^{2+} ionophores for the construction of Zn^{2+} probes are polypyridine derivatives, such as bis(pyridin-2-ylmethyl)amine (BPA), N^1-methyl-N^2,N^2-bis(pyridin-2-ylmethyl)ethane-1,2-diamine (BPEA), N^1-methyl-N^1,N^2,N^2-tris(pyridin-2-ylmethyl)ethane-1,2-diamine (TPEA). These ionophores bind to Zn^{2+} in a 1 : 1 ratio, and the variable coordination number could be used for modulating the Zn^{2+} binding constant of the related probes. On the other hand, 8-aminoquinoline (AQ) of the 2 : 1 Zn^{2+} binding stoichiometry has been widely used in classical Zn^{2+} probes TSQ and analogues (Fig. 20). By incorporating these ionophores with various fluorophores, such as fluorescein or rhodamine, the most well-known Zn^{2+} probes such as ZPs, and ZnAFs (Fig. 20) were prepared.[123,127] For TSQ and analogues, AQ itself acts also as a fluorophore.

4.2.1 Turn-on probes for Zn^{2+} and related design rationales.

With the d^{10} configuration, Zn^{2+} does not quench molecular fluorescence, therefore, the PeT approach (Part 2.1) is more practical for the construction of turn-on probes for Zn^{2+}. The turn-on probes, ZPs and ZnAFs, are all the typical ones based on this approach, and the aforementioned Zn^{2+} ionophores are the emission quenchers, Zn^{2+} coordination to the ionophore only leads to the blockage of PeT from ionophore to fluorophore, which recovers the fluorescence and displays a turn-on response to Zn^{2+}. Cho and co-workers reported a PeT mechanism based two-photon fluorescent Zn^{2+} probe (**SZn-Mito**, **26**) with triphenyl phosphonium (TPP) as the targeting group for mitochondria,[128] BPEA as the ionophore and a naphthalene derivative as the two-photon fluorophore.[129] This probe displays a mitochondria preferential affinity. In MOPS buffer, this probe shows a turn-on (7-fold) fluorescence enhancement to Zn^{2+}, and a maximum two-photon action cross section of 75 GM in the presence of Zn^{2+}. The K_d^{TP} was calculated to be 3.1 (± 0.1) nM. Moreover, it can selectively detect Zn^{2+} in living tissues at a

depth of 100–200 μm without distinct interference from other metal ions. Its two-photon fluorescence contributes to its larger imaging depth than normal fluorescent probes. For TSQ and analogues, the free probes display no emission due to the non-radiative decay by proton transfer *via* intra- and intermolecular hydrogen bonds at the excited state, and the turn-on response is ascribed to Zn^{2+} coordination-induced removal of sulfonamide proton.

4.2.2 Ratiometric probes for Zn^{2+} and related design rationales. Ratiometric Zn^{2+} probes are currently of special interest due to their quantitative imaging ability, and different approaches such as PCT (Part 2.2), ESIPT (Part 2.5) and FRET (Part 2.3) mechanisms are commonly adopted rationales. For the PCT approach, both the acceptor and donor of the ICT fluorophore can be modified as a Zn^{2+} ionophore, We recently reported a mitochondria-targeting ratiometric probe (**Mito-ST**, **27**, Fig. 21) functioning *via* the Zn^{2+} coordination altering the ICT effect of the fluorophore. It consists of a Zn^{2+} ionophore TPEA and an ICT fluorophore 4-amino-7-sulfamoyl-benzo[*c*]-[1,2,5]oxadiazole (SBD) linked with TPP.[130] **27** displays a specific Zn^{2+}-induced hypsochromic shift of both excitation (69 nm) and emission (35 nm) maxima with a K_d of 8.2 (± 0.2) nM. The electron donating 4-amino group was modified as a Zn^{2+} ionophore TPEA, and Zn^{2+} coordination to the donor decreases the HOMO energy of the SBD fluorophore and resulted in a blue-shift of emission and excitation. This probe can be used for monitoring the mitochondrial Zn^{2+} release upon H_2O_2 and SNOC stimulations. The ratiometric Zn^{2+} imaging in MCF-7 cells demonstrated clearly the different mitochondrial Zn^{2+} releasing behavior upon H_2O_2 and SNOC stimulation. This study offers not only a novel reliable and flexible fluorescent agent for the exploration of mitochondria Zn^{2+} homeostasis but also helpful clues for the understanding of ROS/RNS-associated Zn^{2+} biology in mitochondria. However, probes **28**[40] and **29** (NBD-TPEA)[41] developed with a similar approach display no (probe **28**) or very minor (probe **29**, 16 nm) blue-shift of emission (Fig. 21). Their different sensing behavior for Zn^{2+} can be attributed to the photo-disruption of Zn^{2+} in the excited state according to the concept of Valeur,[24] and enhancing the Zn^{2+} binding ability of the ionophore (which is also the donating group) may be helpful to realize the PCT approach for ratiometric probe, just as in the case of **Mito-ST**.

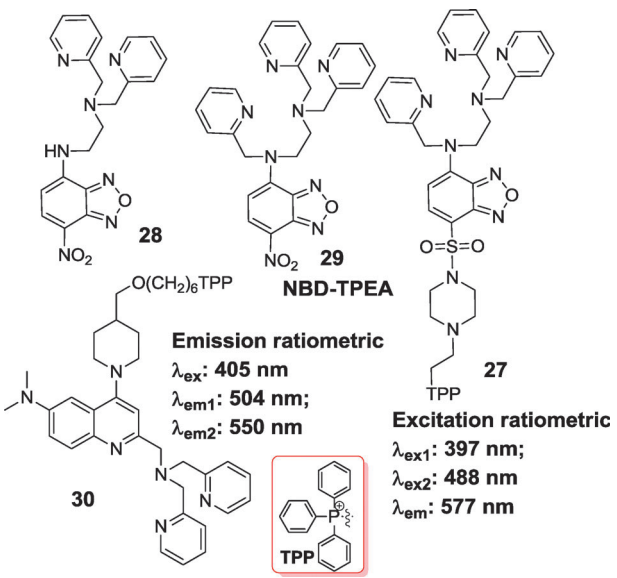

Fig. 21 Chemical structures of Zn^{2+} probes **27–30**.

In Part 2.5 we have shown that the ESIPT approach is also suitable for the construction of ratiometric Zn^{2+} probes, and several probes based on benzimidazole derivatives have been reported. In fact, a ratiometric Zn^{2+} probe with practical intracellular Zn^{2+} imaging ability has also been reported. For example, the probe **30** (**DQZn2**, Fig. 21) reported by Jiang,[131] which is composed of a 4-amino-6-*N*,*N*-dimethylamino quinoline fluorophore, a BPA, and a TPP motif, displays a specific Zn^{2+}-induced emission shift from 550 to 504 nm in HEPES buffer, and a TPP-induced mitochondria-targeting ability. The K_d was calculated to be 0.45 (± 0.01) nM. Its intracellular imaging ability has been proved by the imaging of free mitochondrial Zn^{2+} in NIH3T3 cells. In this probe, the quinoline N and BPA motif act as Zn^{2+} ionophores in a synergic manner, and the quinoline N is protonated in neutral conditions, and the ESIPT process in the free probe can be eliminated by removing the proton from quinoline N *via* Zn^{2+} coordination to the ionophore, which results in a distinct emission hypsochromic shift and enhancement.

Ratiometric Zn^{2+} probes have also been constructed *via* a FRET approach based on fusion proteins. Palmer and co-workers developed two genetically encoded ratiometric Zn^{2+} probes (**ZapCY1**, **31** and **ZapCY2**, **32**, Fig. 22) based on a FRET mechanism by incorporating CFP and citrine into the modified zinc fingers of *Saccharomyces cerevisiae*.[47,132] Zn^{2+} binding by zinc finger motifs of **31** and **32** induces a conformational change in the pair of zinc fingers favoring a FRET process from CFP to citrine. These two probes show highly selective ratiometric response to Zn^{2+} with K_d of 2.5 and 811 pM, respectively. **31** and **32** can target to the endoplasmic reticulum (ER) and Golgi apparatus and allow direct monitoring of Zn^{2+} levels in these structures.

4.2.3 Zn^{2+} probes based on phosphorescent metal complexes. Phosphorescent metal complexes have also been adopted as fluorophores to construct Zn^{2+} probes. For example, Nagano reported a turn-on Zn^{2+} probe, **33**, based on the Eu^{3+}–DTPA complex with a quinoline derivative as a pre-antenna constructed with an approach to the first class of luminescent Ln^{3+} complex-based probes described in Part 3.1.[62] Probe **33** displays a very weak emission in its apo form due to the low efficiency energy transfer from the pre-antenna to Eu^{3+}. Upon addition of Zn^{2+}, it exhibits a Zn^{2+}-induced phosphorescence enhancement due to the increased energy transfer efficiency from the Zn^{2+} coordination-resulting antenna (quinoline/Zn^{2+}) to Eu^{3+}. Due to the long lifetime of phosphorescence of these Ln^{3+} complexes, this Zn^{2+} probe was utilized to improve intracellular Zn^{2+} imaging by the same group *via* time-resolved long-lived luminescence microscopy (TRLLM).[133] With TRLLM, one can eliminate completely the interference of autofluorescence

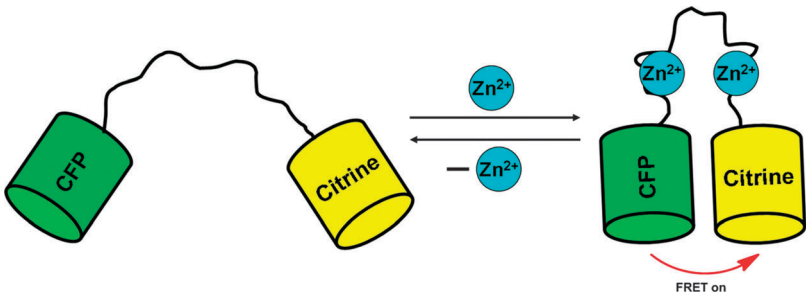

Fig. 22 Schematic diagram of Zn^{2+} sensing mechanism of FRET-based probes **31** and **32**.

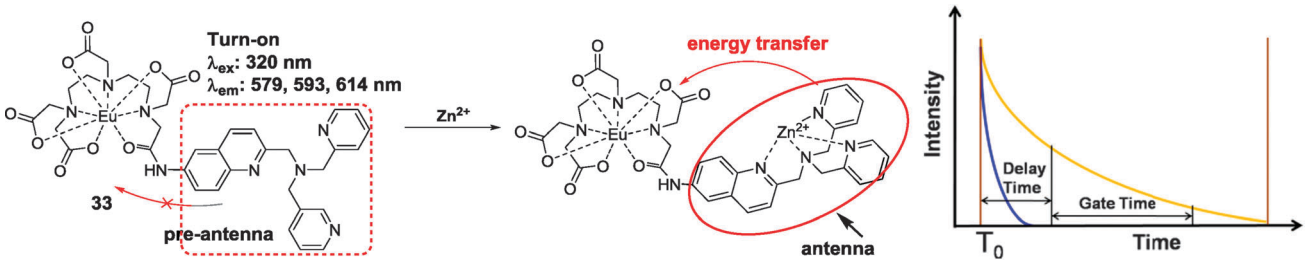

Fig. 23 Left, Eu^{3+} complex-based Zn^{2+} probe **33** and its Zn^{2+} sensing mechanism. Right, the schematic diagram for TRLLM Zn^{2+} detection with a Eu^{3+} complex-based probe. Long-lived luminescence of Eu^{3+} complexes (yellow); short-lived autofluorescence (blue); pulsed excitation light (brown).

of short lifetime and provide high signal-to-noise ratios when an appropriate delay time between the pulsed excitation and detection was applied. The extremely long lifetime (milliseconds) of Eu^{3+} complex phosphorescence is especially favorable to exclude the autofluorescence of the nanosecond-order lifetime (Fig. 23). The intracellular Zn^{2+} imaging of HeLa cells injected with probe **33** demonstrated the ability to track Zn^{2+} inside the cells. Moreover, the low background fluorescence of non-injected cells showed the advantage of this imaging mode.

On the other hand, phosphors based on transition metal complexes can be utilized also to construct Zn^{2+} probes to eliminate the interference of autofluorescence. Cyclometallated iridium(III) complexes with low-lying triplet excited states and lifetimes of around a microsecond are most frequently employed. For example, a new iridium(III) complex (**34**) formed by incorporating a BPA-appended bipyridine ligand shows a Zn^{2+} coordination-induced blue-shift of emission from 640 to 610 nm.[134] Besides the ratiometric sensing behavior, its luminescence lifetime was decreased from 67 to 34 μs. Lo and co-workers reported a series cyclometallated iridium(III) complexes containing the BPA motif for Zn^{2+} detection (Fig. 24).[135] Probes **35–38** exhibit a ^{3}MLCT, ^{3}IL and ^{3}NLCT (triplet amine-to-ligand) induced intense emission in CH_3CN solution (Fig. 24). Upon Zn^{2+} addition, probes **35–38** show Zn^{2+}-coordination induced enhancement of luminescence with enhancement factors of 5.4, 1.6, 1.2 and 4.4, respectively. The K_d values were calculated to be around 10^{-5} M. Recently, Lippard and co-workers reported a novel phosphorescent probe (**39**) for the detection of Zn^{2+} in biological samples (Fig. 24).[74] In this probe, a BPA group was integrated as an ionophore to ligand

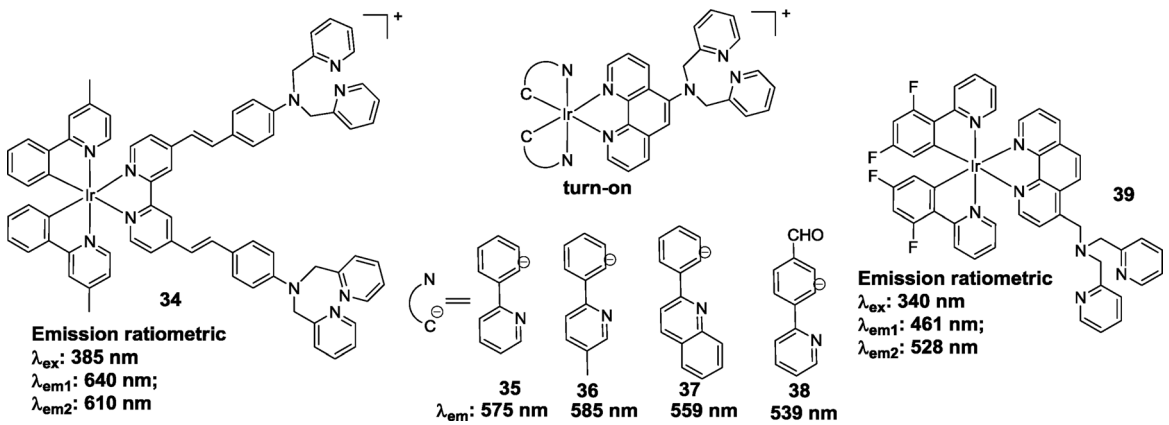

Fig. 24 Chemical structures of probes **34–39**.

1,10-phenanthroline to form the heteroleptic Ir(III) complex. **39** exhibits a dual emission in the blue (461 nm) and yellow (528 nm) regions in its apo form in CH_3CN. Zn^{2+} coordination enhanced the yellow emission band, leading to a ratiometric response. While in PIPES buffer, **39** only exhibits a very weak emission band centered at 520 nm. Addition of Zn^{2+} results in a selective "turn-on" (12-fold) of phosphorescence. This probe displays a 1 : 1 binding stoichiometry with a K_d of 11 nM. The phosphorescent Zn^{2+} detection ability of **39** was applied for live cell imaging in A549 cells. Due to the long lifetime of its phosphorescence, the Zn^{2+}-responsive phosphorescence signals can be separated from total photoluminescence, which allows for the FLIM detection of the Zn^{2+}-induced increase in lifetime in fixed A549 cells.

4.3 Photoluminescent probes for Cu^+/Cu^{2+} and the related design rationales

4.3.1 Turn-on probes for Cu^+/Cu^{2+} and the related design rationales. Due to the paramagnetic nature of Cu^{2+}, its coordination often results in fluorescence quenching of the fluorophore, therefore it is difficult to construct turn-on probe for Cu^{2+} *via* the PeT approach (Part 2.1), and very few systems exhibit fluorescence enhancement with Cu^{2+}especially in aqueous media. The fine tuning of the coordination structure to decrease the paramagnetic nature of Cu^{2+} might be helpful to form turn-on probes, if the related PeT effect in the apo probe is distinct. Although Cu^+ (d^{10} configuration) does not quench fluorescence of organic dyes, it easily disproportionates into Cu^{2+} and Cu^0 in aqueous medium which leads to fluorescence quenching by electron transfer.[136] Therefore, only when the ionophore is able to stabilize the Cu^+ state, is the related Cu^+ fluorescent probe constructed *via* the PeT mechanism able to display a turn-on response. This is also the design principle for a turn-on probe for Cu^+, and the metal coordination set of ionophore for Cu^+ is essential. Cyclic and acyclic aza-thioethers have been found as suitable ionophores for Cu^+ turn-on probes. Fahrni and co-workers reported a 1,3-diarylpyrazoline-based fluorescent probe (**40**) for Cu^+ sensing in PIPES buffer (10 mM, pH 7.2),[137] in which the tetrathia-aza crown ether acts as the Cu^+ ionophore (Fig. 25). This probe shows a 4.6-fold fluorescence enhancement specifically to Cu^+. The association constant of **40** for Cu^+ was calculated to be 7.58 ($\pm$ 1.12) $\times$ 10^6 M^{-1}. Its intracellular Cu^+ imaging ability has been proved in mouse fibroblast cells (3T3). Moreover, its Cu^+-selective imaging ability in living cells has been confirmed by X-ray fluorescence microscopy and X-ray absorption near edge structure (XANES).

By incorporating an acyclic thio-rich ether into various BODIPY dyes, Chang *et al.* have synthesized two turn-on fluorescent probes (**41** and **42**) for Cu^+ (Fig. 25). **41** (**CS1**) exhibits a 10-fold emission enhancement to Cu^+ in HEPES buffer with high selectivity over competitive metal ions of high cellular concentrations.[138] Its membrane-permeability makes it able to be used for the imaging of intracellular Cu^+. Probe **42** (**Mito-CS1**) was constructed by integrating a mitochondria-targeting group TPP with a derivative of **41**.[139] This probe features visible excitation and emission profiles, and a turn-on (10-fold) response to Cu^+ over other examined metal ions. The Job's plot suggests a 1 : 1 binding stoichiometry to Cu^+ with a K_d of 7.2 ($\pm$ 3) pM. Confocal imaging experiments confirmed its specific imaging ability for mitochondrial Cu^+ in living cells. NIR fluorescent Cu^+ probe **43** displays a specific Cu^+-induced 15-fold fluorescence enhancement in HEPES buffer (20 mM, pH 7.0).[140] The Job's plot suggests a 1 : 1 binding stoichiometry between **43** and Cu^+ with an apparent K_d of 3.0 $\times$ 10^{-11} M. The imaging results suggest that **43** can be used for the fluorescent imaging of Cu^+ in living cells. Its NIR excitation/emission nature should facilitate the practical application of **43** for the *in vivo* detection of the labile copper pool in living systems.

On the other hand, the chemodosimeter approach (Part 2.6) *via* the specific Cu^{2+}-induced reaction to form an emissive fluorophore from a non-fluorescent compound is a reliable

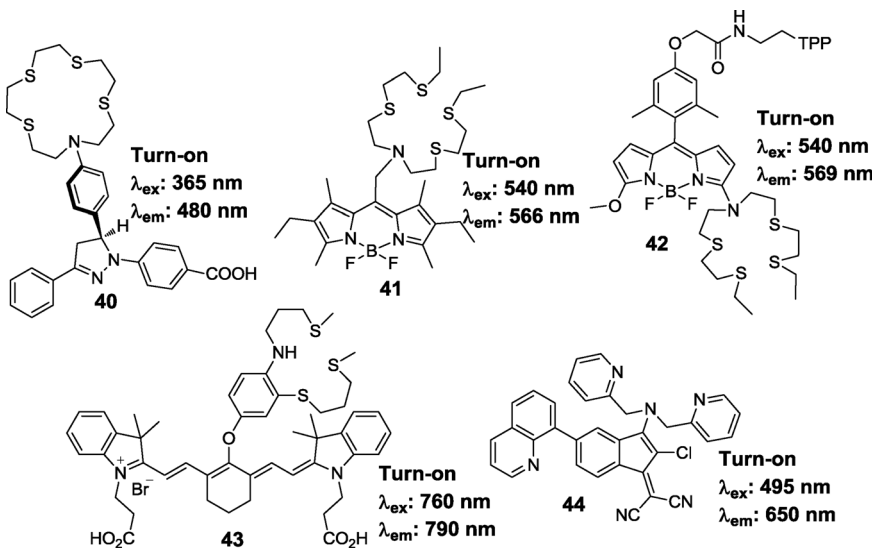

Fig. 25 Chemical structures of turn-on Cu^+ probes **40–44**.

strategy for the construction of turn-on fluorescent Cu^{2+} probes. For example, Cu^{2+} induced ring-opening of xanthene spirolactam derivatives has been developed for this purpose, and the related chemodosimeters have been reviewed recently by Yoon.[56] However, as mentioned in Part 2.6, most of these chemodosimeters display a slow response rate and are irreversible.

A few turn-on Cu^{2+} probes designed based on other mechanisms have also been reported. For example, an quinoline/indene fluorophore hybrid (**44**) was reported as a turn-on fluorescence probe for Cu^{2+}.[141] It exhibits a turn-on sensing behavior towards Cu^{2+} in CH_3CN–H_2O solution with a 1 : 1 binding ratio and a calculated K_a of 1.69×10^5 M^{-1}. The detection limit of a 10^{-4} M solution of **44** for Cu^{2+} in CH_3CN–H_2O was estimated to be *ca.* 4.17×10^7 M.

4.3.2 Ratiometric probes for Cu^{2+}/Cu^{+} and related design rationales. For the design of a ratiometric Cu^{+}/Cu^{2+} probe, the PCT approach (Part 2.2) is always one of the most reliable design rationales, and modifying the electron donating amino group as the Cu^{+}/Cu^{2+} ionophore is the normal method. In this case, Cu^{+} coordination to the ionophore normally leads to a decrease in the HOMO energy, resulting in a hypsochromic shift of excitation or emission. For example, probe **45** is a ratiometric fluorescent Cu^{+} probe derived from an asymmetric BODIPY dye with a 2-acyclic aza-thiaether as the Cu^{+} ionophore, which is also the donor of ICT fluorophore BODIPY (Fig. 26).[142] The free probe displays a dual emission centered respectively at 505 nm (LE band) and 570 nm (ICT band). Upon Cu^{+} addition, it demonstrates a Cu^{+}-induced emission blue-shift from 570 to 556 nm, while the intensity of the emission band at 505 nm remains unchanged. In HEPES buffer, **45** shows a high selectivity for Cu^{+} over other tested metal ions and a *ca.* 20-fold fluorescence ratio change with visible excitation and emission profiles. The calculated K_d for **45** to Cu^{+} is 4.0 ($\pm$ 3) $\times 10^{-11}$ M. Confocal ratiometric imaging results suggest that **45** is capable of sensing the change of intracellular [Cu^{+}]. A similar sensing behavior has been reported for probes **47** and **49** derived from the ICT fluorophore 4,5-disubstituted-1,8-naphthalimide (Fig. 26). In **47**, two 2-(aminomethyl)pyridine ligands were incorporated into the 4,5-positions of 1,8-naphthalimide as a Cu^{2+} ionophore. The addition of Cu^{2+} into the HEPES buffer solution of **47** gives a 1 : 1 Cu^{2+} complex, displaying an emission blue-shift from 525 to 475 nm. The K_a of the **47**/Cu^{2+} complex is 1.35×10^6 M^{-1}.[143] Probe **49** was derived from **47** by replacing one 2-(aminomethyl)pyridine by a hexaethylene glycol motif, showing an improved water solubility over **47**.[144] Upon addition of Cu^{2+}, **49** shows a large emission blue-shift from 534 to 478 nm in HEPES buffer. The Job's plot suggests a 1 : 1 Cu^{2+} binding stoichiometry. The K_a of **49** with Cu^{2+} is 2.7×10^5 M^{-1} (error < 10%). For probe **48**, two 2-(phenylamino)ethylamino groups were introduced to replace the two 2-(aminomethyl)-pyridine motifs of **47** (Fig. 26).[145] **48** shows also a selective

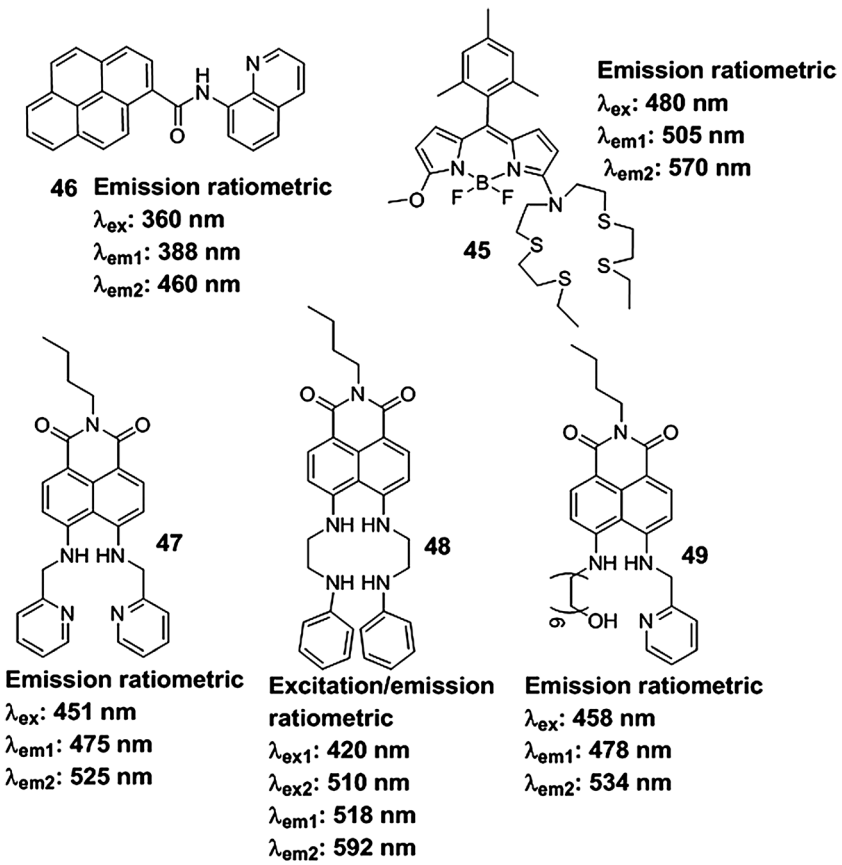

Fig. 26 Chemical structures of Cu^{2+} probes **47–49**.

ratiometric response to Cu^{2+} over other tested metal ions. Although 1 equiv. of Cu^{2+} only leads to an emission quenching of **48** in HEPES buffer, the additional Cu^{2+} induced an emission red-shift from 518 to 592 nm. In this case, the deprotonation of the 4,5-amino group induced by Cu^{2+} coordination enhances the ICT effect of the 1,8-naphthalimide fluorophore and decreases the LUMO energy, resulting in the emission red-shift.

Besides the PCT approach, the excimer approach has also been carried out to construct ratiometric probes for Cu^{+}/Cu^{2+}. The pyrene-based Cu^{2+} probe **46** with 8-aminoquinoline as the ionophore displays a monomer emission at 388 nm (Fig. 26), and its Cu^{2+} coordination with a 2 : 1 stoichiometry induces an excimer emission band centered at 460 nm in CH_3CN.[146] The red-shift from monomer emission to excimer emission exhibits a distinct ratiometric sensing ability for Cu^{2+}. The detection limit of **46** for Cu^{2+} was estimated to be 1.0 μM. The titration profile disclosed a binding constant (K_a) of *ca.* 5.42×10^5 M^{-1}. The naphthalimide-based Cu^{2+} probe (**50**) reported by Spring and Yoon *et al.* shows a selective ratiometric response to Cu^{2+} in HEPES buffer *via* also the excimer mechanism.[147] The piperazine bridge in the free probe prefers a boat-like conformation. This probe displays dual emission bands with the naphthalimide monomer emission (~450 nm) and the excimer emission (~550 nm). Upon addition of less than 1 equiv. of Cu^{2+}, the emission of **50** remains unchanged. However, the addition of a second equiv. of Cu^{2+} induced an enhancement of monomer emission. The switch-on and off of excimer formation triggered by Cu^{2+} has also been confirmed by ^1H NMR analysis and a Job's plot (Fig. 27). The calculated K_a of **50** for Cu^{2+} is about 2.94×10^5 M^{-1}.

A FRET approach is also a valid rationale for the construction of ratiometric probes for Cu^{+}/Cu^{2+}. As discussed in Part 2.3, ratiometric Cu^{2+}/Cu^{+} probes with a FRET mechanism can be constructed based on fused fluorescent proteins, and the bridging peptides or domains between the two fluorescent protein domains are essential for the selective response to Cu^{2+}/Cu^{+}. It is the Cu^{2+}/Cu^{+} coordination to this bridging domain that leads to the change in FRET efficiency and the ratiometric sensing behavior.

4.3.3 Phosphorescent probes for Cu^{2+}/Cu^{+} and related design rationales. Phosphorescent probes for Cu^{2+}/Cu^{+} have also been constructed by luminescent Ln^{3+} complexes and transition metal complexes. The dual-membered sensing system for Cu^{+} showed in Fig. 28 is an excellent example of the sensing approach of an analyte-induced combination of luminescent Ln^{3+} complex and antenna.[148] In this system, the Eu^{3+} complex was tethered with an alkynyl moiety (**51**), while its dansyl fluorophore, with an azide tail (**52**). Therefore, the highly efficient Cu^{+}-catalyzed Huisgen 1,3-dipolar cycloaddition (click reaction) results in the union of the dansyl antenna and europium complex (**53**), which promotes an efficient ISC process between the antenna and Ln^{3+} center and displays a Cu^{+}-triggered 10-fold phosphorescence enhancement.

On the other hand, a phosphorescent transition metal complex has also been utilized to construct a Cu^{2+} probe. You and Lippard developed the first phosphorescent probe (**ZIr2**, **54**) for ratiometric detection of Cu^{2+} *via* combining a heteroleptic Ir(III) complex with dual emission bands and a long lifetime with a BPA ionophore.[149] Free **54** displays a dual phosphorescence, green emission of ppy ligands (470–570 nm, Ippy) and red emission of the Ibtp ligand (580–700 nm, Ibtp). Addition of Cu^{2+} results in quenching of the red emission, and the enhancement of the intensity ratio of green emission to red emission was *ca.* 4-fold. **54** exhibits an excellent reversibility and selectivity for Cu^{2+}, with a K_d of 16 μM. Intracellular copper ion imaging was also achieved by using the ratio of phosphorescence signals acquired through green and red channels. For this heteroleptic complexes, Cu^{2+} coordination to the BPA ionophore tethered to the Ibtp ligand will alter the MLCT state related to Ibtp and decrease the related emission, while the emission related to ppy is almost intact, displaying the ratiometric sensing behavior.

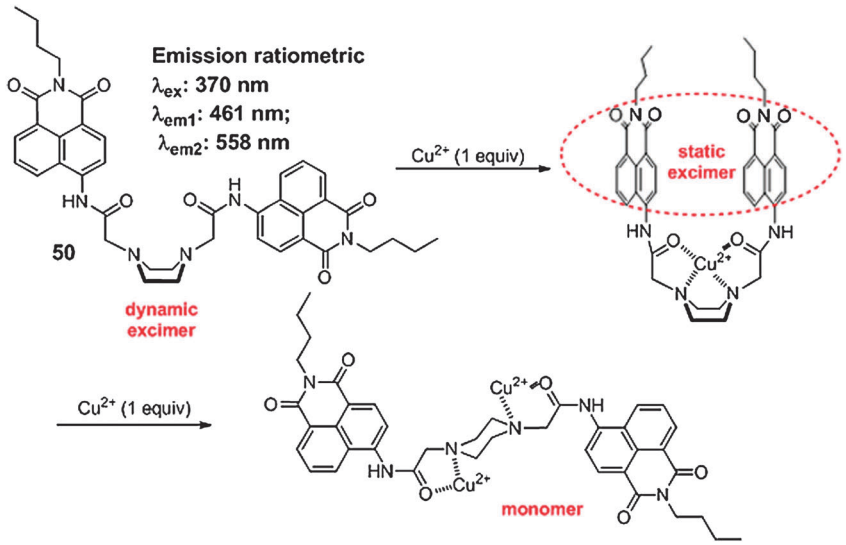

Fig. 27 Proposed mechanism of stepwise binding mode of **50** with Cu^{2+}.

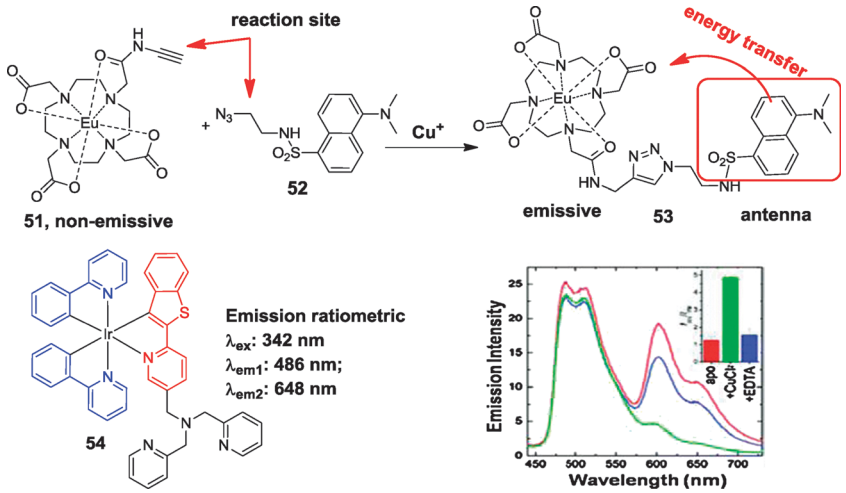

Fig. 28 Top: the dual-membered Cu^{2+} sensing system composed of compounds **51** and **52** and its sensing mechanism. Bottom: structure of phosphorescent probe **54** and its phosphorescent spectra in the presence or absence of Cu^{2+}.

4.4 Photoluminescent probes for hazardous Hg^{2+} and Cd^{2+} and the related design rationales

4.4.1 Turn-on photoluminescent Hg^{2+} probes and related design rationales. The design of fluorescent probes for heavy metal ions such as Hg^{2+} and Cd^{2+} remains a hot field because of their interests for chemistry, biology, and environmental science. A large number of fluorescent probes have been reported in recent years, and have been reviewed extensively.[13,36] As a heavy metal ion, Hg^{2+} coordination usually induces the quenching of luminescence. Therefore, the normal PeT approach (Part 2.1) does not always work for the construction of turn-on probes for Hg^{2+}. As a typical soft acid, Hg^{2+} has a high affinity for soft and even borderline Lewis bases including thiols, thioethers and pyridine. Therefore, sulfur-rich ionophores are most used for the reverse sensing of Hg^{2+}.[150] In order to avoid Hg^{2+}-induced luminescence quenching, specific Hg^{2+}-induced reactions were adopted for the design of turn-on Hg^{2+} chemodosimeters (chemodosimeter approach, Part 2.6). For example, several Hg^{2+} chemodosimeters have been designed *via* desulfurization followed by cyclization (**55–57**),[151–153] and thioacetal deprotection (**58**, Fig. 29).[154] Utilizing Hg^{2+}-induced umpolung reaction mechanisms, Hg^{2+}-selective chemodosimeters with turn-on and/or ratiometric sensing behavior can be achieved. It should be noted that fluorescent response of normal organic dyes is normally solvent-dependent, and probes for Hg^{2+} in aqueous solutions are especially appreciated.

Turn-on Hg^{2+} probes constructed with the PeT approach are more attractive, since they normally display instant and reversible Hg^{2+} sensing ability. A few examples of this kind of probe have also been reported. By introducing an azathiocrown ether ionophore to the TPAN fluorophore, Cho *et al.* designed a two-photon fluorescent probe (**59**) for Hg^{2+} sensing (Fig. 30).[155] This probe can be excited by 780 nm femto-second pulses and shows a "turn-on" (6-fold) response to Hg^{2+} in aqueous solution with a K_d^{OP} of 0.46 (± 0.01) μM and K_d^{TP} of 0.45 (± 0.01) μM, respectively. With high photostability and negligible toxicity, **59** can visualize Hg^{2+} accumulation in fresh fish organs using two-photon microscopy. In this case, the spacer between the azathiocrown ether and TPAN fluorophore should be helpful to decouple the spin–orbit interactions and remove the emission quenching effect of Hg^{2+}, therefore, the Hg^{2+} coordination to the ionophore only displays the PeT blocking effect and results in the turn-on response. A similar case was also observed for probe **60** (**NBD-TAEE**, Fig. 30), which displays a specific Hg^{2+}-induced emission enhancement (~29-fold).[156] However, its analogue without the ethylene spacer between the ionophore and NBD fluorophore shows no turn-on response to Hg^{2+}.

4.4.2 Ratiometric photoluminescent Hg^{2+} probes and related design rationales. Similar to the case of turn-on probes, ratiometric Hg^{2+} probes also can be constructed *via* specific Hg^{2+}-induced reaction altering the ICT effect of an ICT fluorophore. Probe **61** is a Nile blue-based chemodosimeter with a nanomolar detection limit for Hg^{2+} in 100% aqueous solution.[157] Mixing with aqueous Hg^{2+} solution, a considerable blue-shift in its absorption and emission spectra was observed, which was ascribed to the Hg^{2+}-triggered desulfurization reaction shown in Fig. 29. The Hg^{2+} promoted formation of 2,5-dihydro-1*H*-imidazol-2-amine altered the ICT effect of the fluorophore, resulting in the emission shift from 652 to 626 nm.

With the good water solubility and high Hg^{2+} affinity of Cys residues, Lee and co-workers developed a ratiometric fluorescent probe (**62**) for Hg^{2+} in aqueous solution composed of two dansyl fluorophores linked by dimerized Cys residues.[158] The probe features high sensitivity and selectivity to Hg^{2+}. Both "turn-on" and ratiometric responses were observed with a K_d of 41 nM. Hg^{2+} addition leads to a hypsochromic shift from 541 to 507 nm. Its low detection limit (1.6 ppb) matches the maximum allowable level (2 ppb) of Hg^{2+} in drinking water established by the US EPA. The exact reason for the ratiometric sensing ability of **62** is still not clear, yet the Hg^{2+} coordination-induced deprotonation of sulfonamide has been verified, therefore, the Hg^{2+} coordination blocked ESIPT might be the origin.

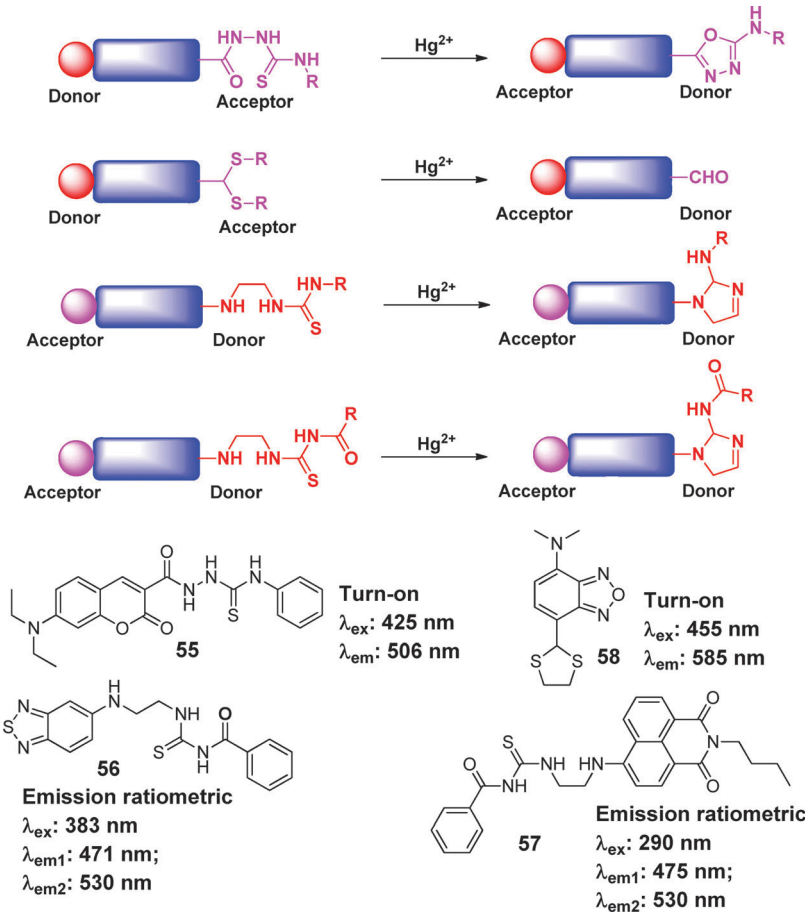

Fig. 29 Hg^{2+}-induced reactions for chemodosimeter design and related Hg^{2+} probes **55–58**.

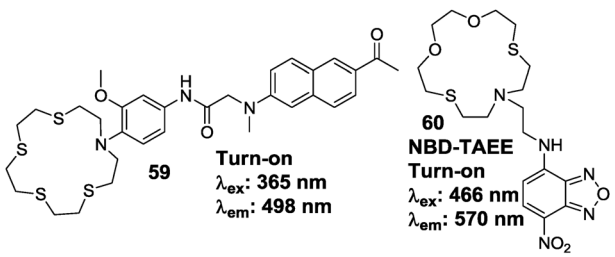

Fig. 30 Chemical structures of turn-on Hg^{2+} probes **59** and **60**.

On the other hand, a ratiometric probe for Hg^{2+} can also be developed with the excimer approach (Part 2.4). For example, Yao *et al.* reported a new pyrene-based derivative (**63**) as a ratiometric probe for Hg^{2+} in aqueous solution (Fig. 31).[159] Probe **63** exhibits a very weak monomer emission at around 395–410 nm. After binding to Hg^{2+}, an intense excimer emission of pyrene centered at 462 nm appears. This dual emission sensing behavior makes **63** a practical ratiometric probe for Hg^{2+}. The effective π coordination of Hg^{2+} to pyrene favoring excimer formation is the origin of the ratiometric sensing mechanism.

4.4.3 Photoluminescent Cd^{2+} probes and related design rationales. In the case of Cd^{2+}, most efforts have been concentrated on how to increase the selectivity of the receptor for Cd^{2+}.[36] The normal ionophores for Cd^{2+} are BPA, quinoline, polyamine and their derivatives. Due to the similar coordination properties to Zn^{2+}, Cd^{2+} coordination usually causes a similar fluorescent response, and the discrimination of Cd^{2+} from Zn^{2+} in fluorescence sensing is still very challenging, and fluorescent Cd^{2+} probes with no interference from Zn^{2+} are highly desirable. In fact, fine tuning the metal coordination sphere of the ionophore to enhance the selectivity for Cd^{2+} is still tricky.

Cd^{2+} does not quench molecular fluorescence of the fluorophore due to its d^{10} electron configuration. Therefore, the PeT approach is a practical rationale for the design of turn-on Cd^{2+} probes. A two-photon excitable fluorescent probe (**64**) for Cd^{2+} based on a naphthalene fluorophore has been reported (Fig. 32).[160] This probe exhibits a turn-on response to Cd^{2+} in Tris–HCl buffer solution. The turn-on sensing behavior of **64** originated from a Cd^{2+} coordination blocked PeT process from the chelator to the fluorophore. The calculated K_d was 6.1×10^{-5} M for the one-photon mode and 7.2×10^{-5} M for the two-photon mode, respectively. Its two-photon Cd^{2+} imaging ability has been proved in living HepG2 cells.

Similar to the case of Zn^{2+} sensors, the PCT approach (Part 2.2) is also the most important rationale to design ratiometric Cd^{2+} probes.

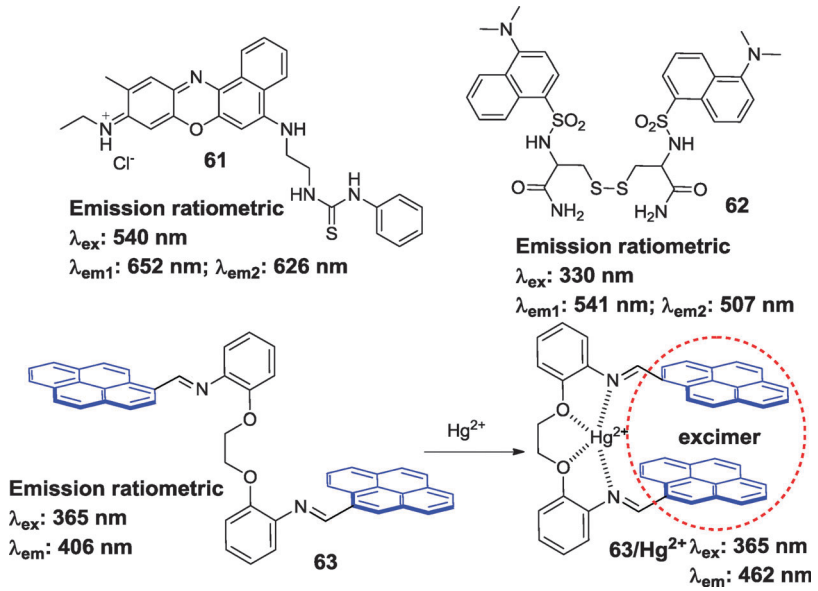

Fig. 31 Ratiometric Hg^{2+} probes **61–63** and the Hg^{2+} sensing mechanism of probe **63**.

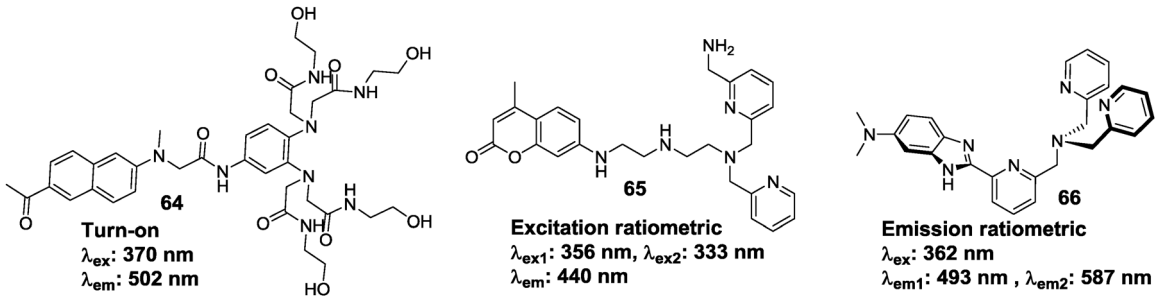

Fig. 32 Chemical structures of Cd^{2+} probes **64–66**.

For example, the ratiometric probe **65** is composed of coumarin-120 (C120) and a Cd^{2+} chelator derived from *N*,*N*,*N*′,*N*′-tetrakis-(2-pyridylmethyl)ethylenediamine (TPEN), a general cell membrane permeable chelator for transition metal cations (Fig. 32).[161] This probe exhibits an excellent selective ratiometric response to Cd^{2+} over other transition metal ions showing a hypsochromic excitation shift from 356 to 333 nm. The Cd^{2+} coordination to the 7-amino derived ionophore can decrease the HOMO of the coumarin fluorophore and decrease the ICT effect of coumarin, which is the origin of this ratiometric sensing behavior. This probe shows also a strong binding ability (K_d = 0.16 nm) and low detection range (40–660 pM) for Cd^{2+}. The ratio imaging experiments demonstrate that **65** can be a useful tool for detecting [Cd^{2+}] fluctuation in living mammalian cells.

We have also reported a ratiometric probe (**66**, DBITA) for Cd^{2+} based on metal chelation induced co-planation of a 2,2′-azo-1,1′-biaryl fluorophore (Fig. 32).[162] This probe features a large Cd^{2+}-induced red emission shift (53 nm) from 493 to 534 nm in HEPES buffer. The Cd^{2+} coordination-induced co-planation of the fluorophore enlarges the conjugated aromatic system (which is also an ICT fluorophore) and decreases the gap between the LUMO and HOMO, and finally results in the bathochromic shift of emission. It exhibits a large Stokes' shift and high quantum yield and can be utilized to detect Cd^{2+} at the picomolar level. Confocal imaging experiments indicated that **66** can be used for monitoring Cd^{2+} levels in living cells.

5. Metal coordination in fluorescent sensing of anions and neutral molecules

5.1 Fluorescent probes for PPi, ATP favored by metal coordination

Among the metal ion complexes utilized as PPi binding units, BPA/Zn^{2+} and BPA/Cu^{2+} complexes and their analogs have been studied extensively. Some recent examples are given as follows.

5.1.1 Turn-on probes for PPi and the related metal coordination-based approaches. As shown in Fig. 33, PPi probes with turn-on responses were developed *via* two different strategies: PPi coordination and PPi induced decopperization. In the first case, two BPA/Zn^{2+} subunits are incorporated into a fluorophore through a spacer. The distance between the two

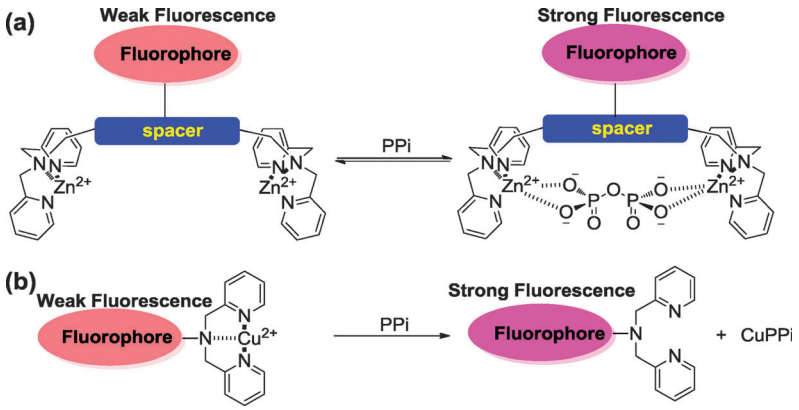

Fig. 33 Turn-on fluorescent sensing mechanisms for PPi based on fluorescent Zn^{2+} or Cu^{2+} complexes. (a) PPi coordination and (b) PPi induced decopperization.

BPA/Zn^{2+} motifs can be tuned by the spacer. In the absence of PPi, the probes display very weak fluorescence due to the effective PeT process from BPA to the fluorophore, since at least the BPA binding of the second Zn^{2+} is not favored by the electrostatic repulsion between two Zn^{2+} centers. In the presence of PPi, a distinct fluorescence enhancement is observed, since the synergic coordination of PPi with two BPA motifs to both Zn^{2+} centers, together with the decreased electrostatic repulsion due to the negative charge of PPi, favors the effective binding of both Zn^{2+} centers by BPA, and the PeT effect from BPA to the fluorophore can be blocked effectively. Therefore, this sensing mechanism is still a PeT approach (Part. 2.1).

With this approach, Hong and co-workers have developed a TPE–BPA–Zn^{2+} based fluorescence probe (**67**) which exhibits turn-on sensing behavior upon binding with PPi in aqueous solution (Fig. 34).[163] This probe shows a mild sensitivity and selectivity for PPi over AMP and ATP. The PPi addition results in a 12-fold fluorescence enhancement. Its detection limit for PPi was estimated to be 0.90 μM according to fluorescence titration. Yoon *et al.* reported a BPA/Zn^{2+} based fluorescence probe (**68**) for PPi by integrating a bis(BPA/Zn^{2+}) unit to a fluorescein moiety (Fig. 34).[164] **68** shows a highly selective and sensitive turn-on response towards PPi in 100% aqueous solution with a K_a of 9.8×10^7 M^{-1}. Its PPi binding in aqueous solution demonstrates a slight red shift of emission (~13 nm) and a synergic chelation enhanced fluorescence (~1.5 fold). The red shift of emission could be attributed to altered Zn^{2+} coordination to the phenolate oxygen of fluorescein.

The bis(BPA/Zn^{2+})–phenoxide system has been proved to be a promising receptor for PPi binding in aqueous systems.[165] Hong *et al.* extended this receptor to a fluorescent probe (**69**) for the detection of PPi (Fig. 34).[166] This probe is a naphthalene-based bis(BPA/Zn^{2+})–phenoxide probe, which exhibits highly selective turn-on sensing behavior (9.5-fold) towards PPi in HEPES buffer. The K_a for PPi was calculated to be 2.9×10^8 M^{-1}. Moreover, **69** is able to detect less than 1 equiv. of PPi in the presence of a 50- to 250-fold excess of ATP. We reported also a visible light excited fluorescent PPi probe (**70**) which was constructed by appending a BPA–Zn^{2+} unit to an ICT fluorophore 4-amino-7-sulfonyl-2,1,3-benzoxadiazole (ASBD, Fig. 34).[167] **70** displays a selective PPi induced fluorescent turn-on response upon excitation at 468 nm in HEPES buffer. The fluorescence enhancement induced by PPi binding is around 5-fold. The K_a of **70** with PPi was estimated to be 4.1×10^5 M^{-1}.

For a second type of turn-on probe for PPi based on a decopperization approach, weakly bound Cu^{2+} ions can be removed from the probe upon addition of PPi due to the formation of PPi/Cu^{2+} complexes, and the emission quenching effect of Cu^{2+} is eliminated, resulting in the fluorescence enhancement. With this approach, a naphthalimide–BPA/Cu^{2+} based PPi probe (**71**) was developed and immobilized onto mesoporous silica (Fig. 35).[168] This probe shows a high and

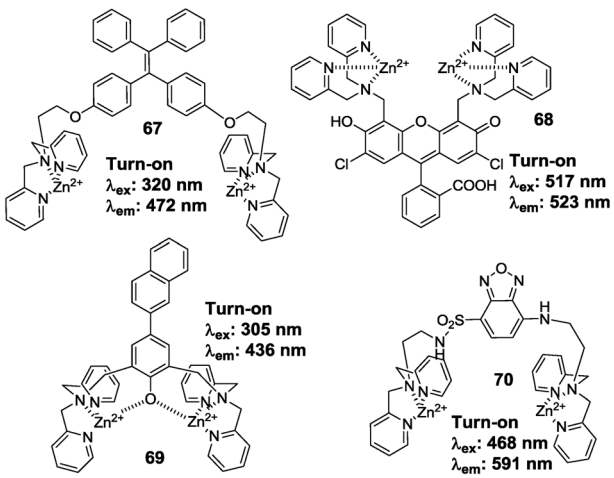

Fig. 34 Chemical structures of fluorescent PPi probes **67–70**.

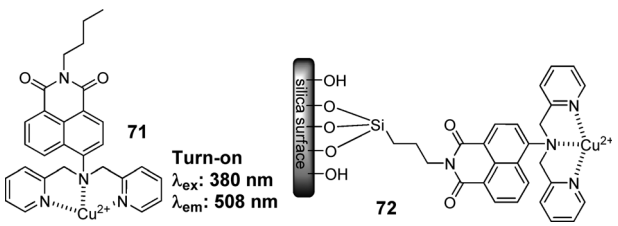

Fig. 35 Structures of fluorescent probes **71** and **72** for PPi.

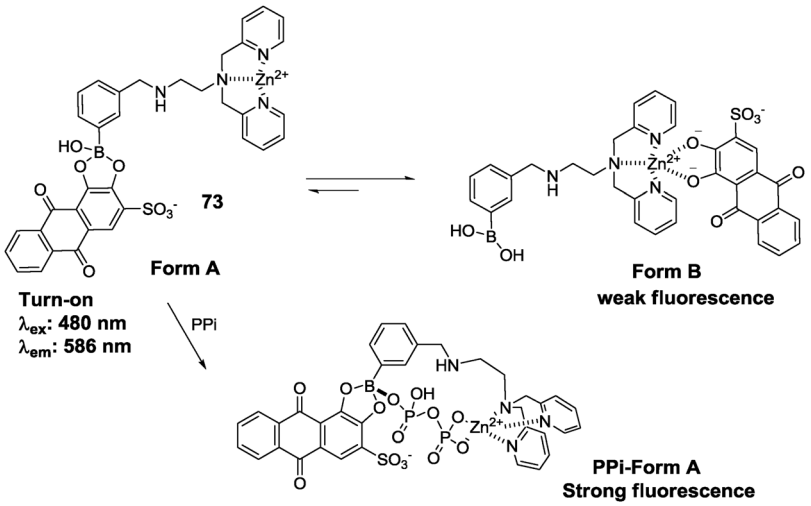

Fig. 36 Proposed sensing mechanism for PPi fluorescent probe **73**.

selective turn-on sensing behavior towards PPi (6-fold), which is attributed to the PPi induced decopperization process. The immobilized probe **72** exhibits a quick response (~100 s) and a large fluorescence enhancement (~10-fold) for PPi. The detection limit was estimated to be 10 ppb.

Kubo and co-workers employed a specific anion replacement strategy to devise a new probe for the detection of PPi in aqueous solution (Fig. 36).[169] BPA–Zn^{2+} appended phenylboronic acid and alizarin dye can self-assemble to form two different forms in MeOH–HEPES buffer, and the mixing system of form A (**73**) and form B exhibits weak fluorescence. Upon addition of PPi, a boronate ester can be formed between PPi and **73**, resulting in an emission enhancement. Moreover, **73** shows a high selectivity for PPi over ATP, ADP, AMP and other tested anions. The K_a of **73** with PPi was estimated to be $(1.6 \pm 0.04) \times 10^6$ M^{-1}, which is 10-fold and 84-fold higher than those for ATP and ADP, respectively. The boronate ester formation and Zn^{2+} coordination functions in a synergic manner and favors the stability of PPi–Form A which is the origin for this sensing behavior.

5.1.2 Ratiometric probes for PPi and the related metal coordination-based approaches. Most reported ratiometric probes for PPi have been constructed *via* an excimer formation approach (Part 2.4). In the absence of PPi, these sensing systems usually display a monomer emission of short wavelength. The synergic binding of PPi with two BPA/Zn^{2+} motifs tethered to two fluorophores favors the π–π interaction between fluorophores to form the excimer upon excitation, which displays the excimer emission and a red shift of emission can be observed (Fig. 37). For example, Hong and co-workers reported a pyrene–BPA/Zn^{2+} based fluorescent probe (**74**) (Fig. 38) for PPi.[170] In its apo form, **74** shows a very weak monomer emission of pyrene (360–450 nm). After binding with 2 equiv. PPi, the **74**/PPi complex exhibits a strong excimer emission band centered at 475 nm. It is able to detect PPi selectively in the presence of 10 equiv. of ATP. The naphthaldiimide–BPA/Zn^{2+} based fluorescent probe (**75**) reported by Yoon and co-workers is able to sense PPi in pure aqueous solution.[171] The unique excimer peak at 490 nm can be observed only in the presence of PPi due to the PPi-favored π–π interaction inducing the formation of a unique [2 + 2] excimer. The calculated K_a for PPi is 4.1×10^5 M^{-1}. The naphthalene–tetrazamacrocycle–Zn^{2+} based fluorescent probe (**76**) reported by Wang and co-workers displays a selective PPi induced emission shift from the monomer emission (337 nm) to the excimer emission (415 nm) over Pi, PO_3^{3-}, ADP, AMP and ATP. The K_a of the **76**/Zn^{2+}/PPi complex was estimated to be 2.1×10^8 M^{-1}.[172]

The ESIPT approach (Part 2.5) has also been reported to design a ratiometric probe for PPi. The bis(BPA/Zn^{2+})-bearing

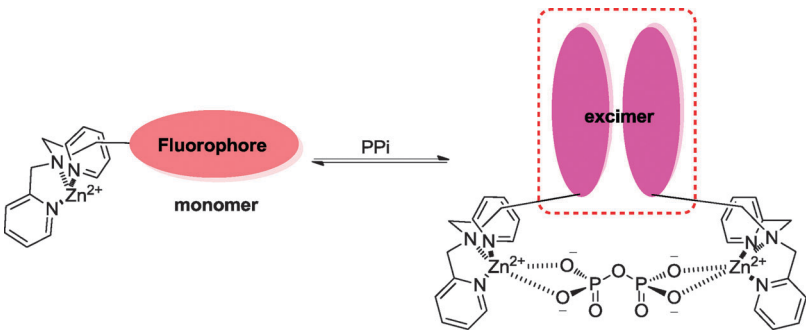

Fig. 37 Schematic diagram of ratiometric sensing mechanism of fluorescent probes for PPi *via* excimer formation.

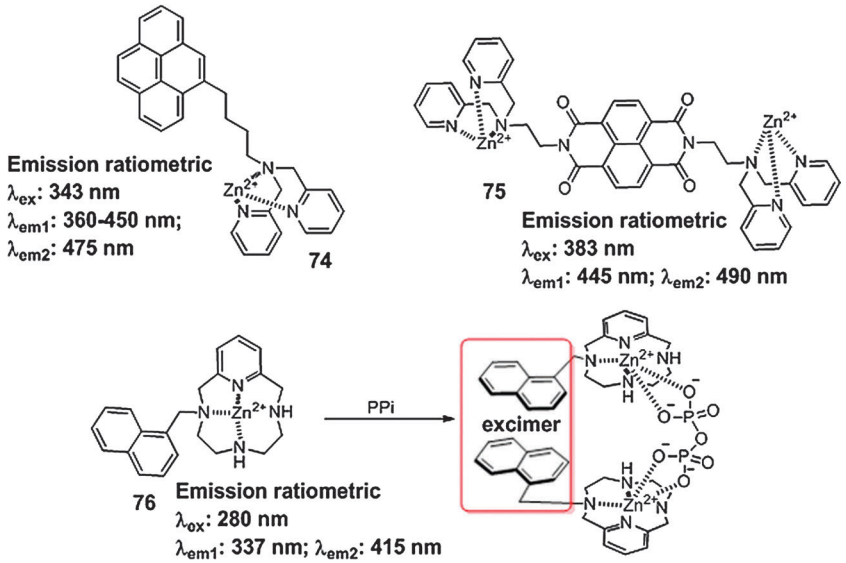

Fig. 38 Ratiometric fluorescent probes **74–76** for PPi based on excimer formation.

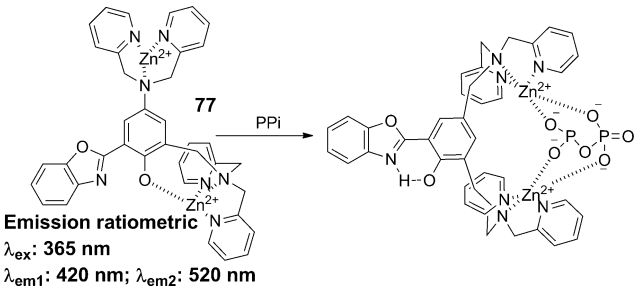

Fig. 39 Proposed mechanism of ratiometric fluorescent probe **77** for PPi sensing.

ratiometric fluorescent probe (77) reported by Pang and co-workers shows highly selective binding for PPi over the other structurally similar phosphate ATP and related anions displaying a PPi induced bathochromic emission shift from 420 to 520 nm (Fig. 39).[173] In the absence of PPi, the phenol proton is removed by Zn^{2+} coordination and the resulting phenoxide participates in Zn^{2+} coordination in a synergic manner with the BPA motif. In the presence of PPi, PPi coordinates to two Zn^{2+} centers simultaneously with two BPA motifs, and recovers the phenol form. Therefore, the ESIPT process can be realized in the final product which results in a large emission bathochromic shift. The ESIPT turn-on mechanism is supported by ^{1}H NMR determination and molecular modeling.

5.1.3 Probes for ATP and the related metal coordination-based approaches. For the construction of turn-on fluorescent probes, a similar synergic Zn^{2+} coordination approach to the turn-on PPi probe can be utilized. The turn-on fluorescent ATP probe **78** developed by Hamachi and co-workers consists of a bis(BPA/Zn^{2+}) unit as the receptor and xanthene as the fluorophore (Fig. 40).[174] This probe selectively senses ATP with a large emission enhancement (EEF > 15) and strong binding affinity (K_{app}, 1×10^6 M^{-1}). It is suggested that activated water by synergic coordination to the two Zn^{2+} centers could attack the *meso*-carbon atom of xanthene in a nucleophilic manner which quenches the emission of xanthene. The conjugated form of xanthene can be recovered from its de-conjugated form upon ATP binding, which results in a turn-on of emission. In addition, the synergic Zn^{2+} coordination of BPA and ATP should also contribute to the high emission enhancement *via* the enhanced blockage of the PeT effect from BPA to the fluorophore. The bioimaging ability of **78** has been demonstrated by confocal fluorescence imaging of ATP in living cells.

Other approaches for turn-on ATP probes have also been reported. Integrating a BPA/Zn^{2+} system as the receptor with two-photon fluorophore 6-acetyl-2-(dimethylamino)naphthalene (Acedan) resulted in a two photon fluorescence (TPF) probe (**79**) for ATP and ADP (Fig. 41).[175] This probe can selectively detect ATP and ADP in aqueous solution *via* displaying a turn-on response. Fluorescence and ^{1}H NMR titrations suggest that Zn^{2+} coordination and π–π interactions between the fluorophore and nucleobase functioning in a synergic manner are responsible for the selective response. Since **79** is cell membrane permeable, it can be applied for two-photon imaging of ATP and ADP in living cells. Duan and co-workers reported a Co^{2+} complex (**80**) formed by a ligand bearing a dansyl group displays a size-selective turn-on (4-fold) fluorescence response to ATP in aqueous solution *via* electrostatic interactions between this Co^{2+} complex and ATP (Fig. 41).[176]

Two ratiometric probes (**81** and **82**) for ATP have been developed with the FRET approach. The two FRET-based ratiometric probes were constructed by integrating a coumarin fluorophore as **D-F** with **78** as **A-F** (Fig. 42).[177] The FRET efficiency of these two probes can be modulated *via* the ATP-altered spectral overlap, since the synergic ATP coordination to both Zn^{2+} centers with two BPA motifs can recover the conjugated xanthene fluorophore from the de-conjugated (non-fluorescent) form. Both probes exhibit a significant emission

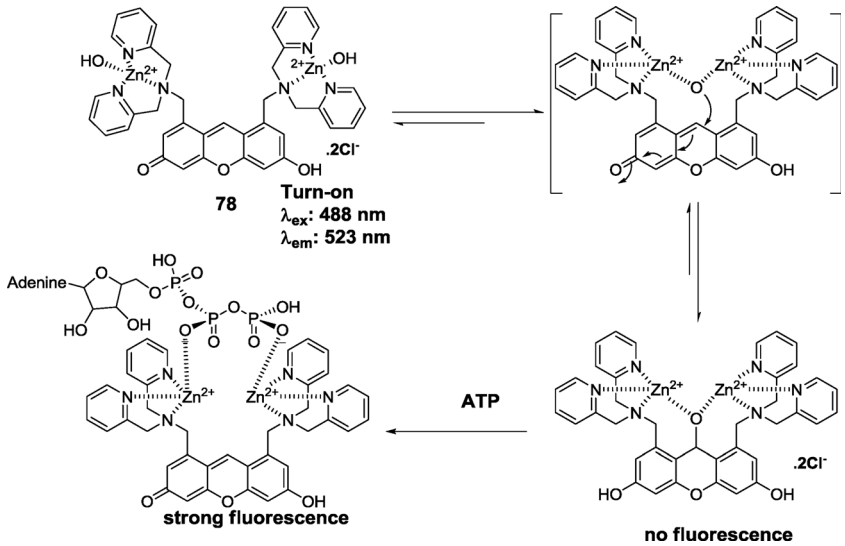

Fig. 40 Schematic diagram of turn-on fluorescent sensing mechanism of **78** for ATP.

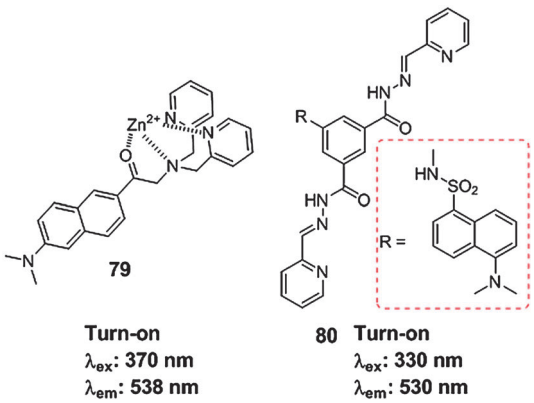

Fig. 41 Fluorescent probes **79** and **80** for ATP.

ratio change with strong binding affinity (K_{app}, 10^6–10^7 M^{-1}) to ATP in aqueous solution. **81** and **82** were successfully applied in the real-time fluorescence monitoring of ATP-involved enzyme reactions and ratiometric ATP imaging in living cells.

5.2 Paramagnetic metal complex-based fluorescent probes for nitric oxide (NO) and nitroxyl (HNO)

Fluorescent sensing of NO in real time and *in vivo* has gained great attention in the fields of biology, chemistry and medical sciences.[178,179] NO sensing can be realized by interacting NO with metal complexes of fluorescent ligands (fluorophores). Lippard and co-workers reported several metal complexes as fluorescent nitric oxide probes with three different sensing mechanisms including fluorophore displacement, Cu^{2+} reduction by NO, and ligand nitrosation. All the three mechanisms are based on the emission quenching effect of a paramagnetic metal center in free metal complex probes, the turn-on response to NO was realized *via* NO-induced metal center reduction to the d^{10} configuration, which no longer quenched the emission of the fluorophore ligand, or *via* NO-induced removal of metal center.

As shown in Fig. 43a, probe **83** does not exhibit any fluorescence due to Co^{2+}-coordination and π–π stacking between two dansyl groups.[180] However, it displays a turn-on response upon

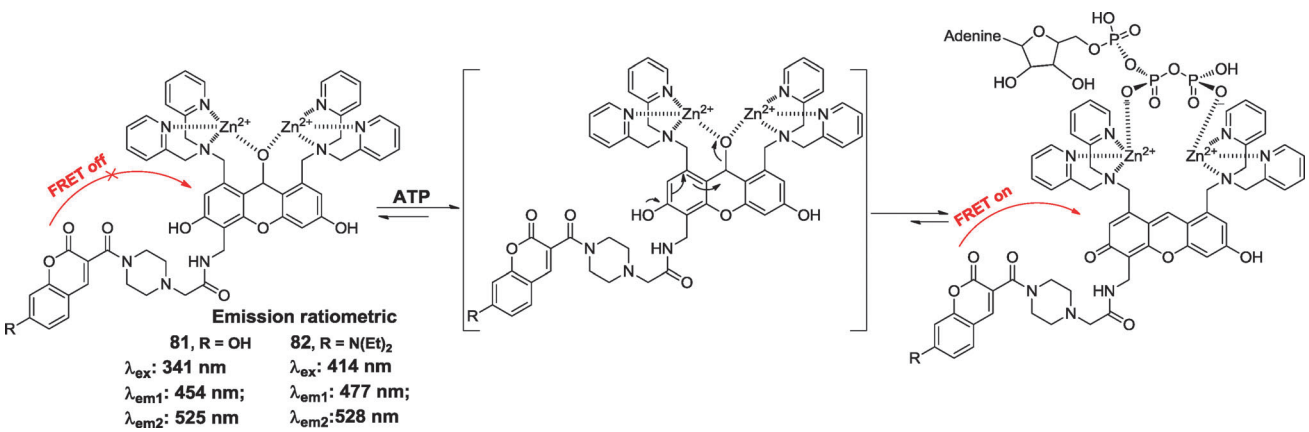

Fig. 42 Schematic diagram of dual-emission sensing of ATP with **81** and **82**.

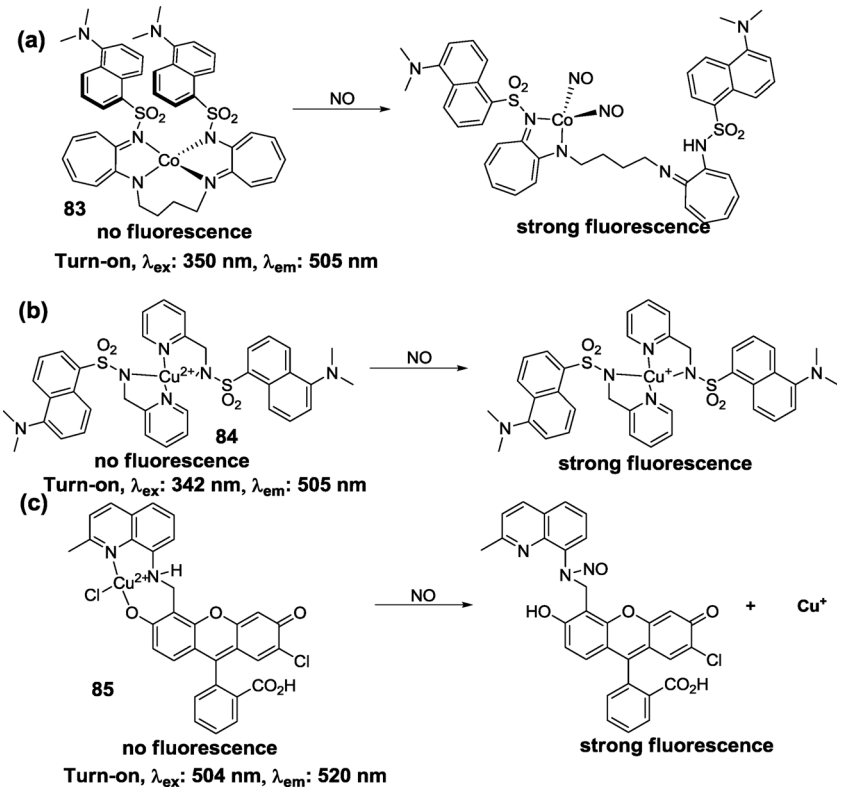

Fig. 43 Different NO sensing mechanisms of NO probes **83–85**.

NO addition due to the formation of a Co–NO complex with d^{10} configuration and the disruption of the excimer. This mechanism can be only achieved in organic solvents due to the competitive H_2O coordination. Similarly, Cu^{2+} complex-based probe **84** shown in Fig. 43b exhibits no emission due to the quenching effect of the paramagnetic Cu^{2+} center.[181] Its fluorescence can be turned on when binding to NO which reduces Cu^{2+} to Cu^{+} of d^{10} configuration. However, probes based on this mechanism have difficulty in sensing NO in physiological conditions. In the case of fluorescein-based **85** (Fig. 43c), an NO-triggered fluorescence increase can be observed *via* Cu^{2+} reduction to Cu^{+} accompanied by the concomitant dissociation of the *N*-nitrosated fluorophore ligand from Cu^{+}.[182]

Nitroxyl (HNO) is a one-electron reduced, protonated analogue of NO, displaying important biological roles in pharmacological applications different from those of nitric oxide.[183] A similar approach for paramagnetic metal complex-based NO probes has been adopted to construct HNO probes. Recently, two trizole–BPA–Cu^{2+}-based probes (**86** and **87**) for HNO were reported (Fig. 44).[184,185] These probes function in biological conditions *via* an HNO-induced reduction of Cu^{2+} to Cu^{+}. Probe **86** is the first fluorescent probe reported for HNO detection in living biological samples with visible excitation and emission, in which the BDP fluorophore is linked to a trizole–BPA–Cu^{2+} unit. It features a 4-fold fluorescence enhancement in aqueous solution upon HNO addition, and displays a high HNO selectivity over other NO analogues. Although its fluorescence can be recovered by cysteine treatment due to the reduction of Cu^{2+}, fluorescence imaging in HeLa cells suggest that normal intracellular levels of cysteine and other thiols is insufficient to interfere with its fluorescent response to HNO. By introducing a coumarin fluorophore to a trizole–BPA–Cu^{2+} unit, **87** shows 17-fold fluorescence enhancement with HNO, which is much higher than **86**.

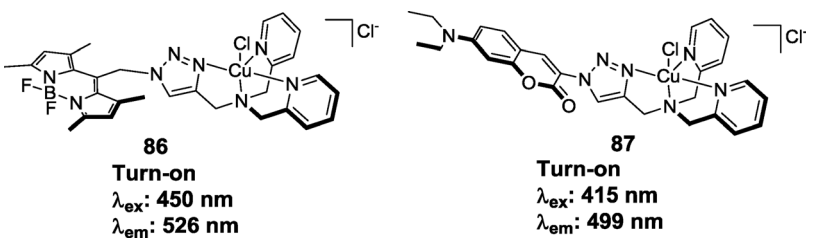

Fig. 44 Chemical structures of HNO probes **86** and **87**.

5.3 Paramagnetic metal complex-based fluorescent probes for hydrogen sulfide (H_2S)

H_2S is closely associated with several biological progresses, and has been identified as the third biological gasoneurotransmitter following nitric oxide (NO) and carbon monoxide (CO).[186–189] Therefore, the development of fluorescent probes for biological H_2S sensing is crucial for the understanding of biological functions of H_2S. Since most endogenous H_2S undergoes dissociation in physiological medium of pH 7.4, either H_2S, HS^- or S^{2-} can be analytes for sensing. Most reported H_2S probes were designed based on two major approaches, *i.e.* H_2S-induced reaction to alter the fluorescence of conjugated fluorophores, and H_2S-induced removal of an emission quenching metal center by S^{2-} from the fluorescence quenched complexes. Since the second approach leads to a quicker turn-on response than the first one, it has been frequently adopted for the probe design. Since Cu^{2+} displays a distinct emission quenching effect due to its paramagnetic nature, Cu^{2+} is the mostly used paramagnetic metal to construct H_2S probes with fluorescent ligands, profiting also from its high S^{2-} affinity to favor Cu^{2+} removal.

Sulfide probe **88** reported by Chang's group is a fluorescein-based BPA–Cu^{2+} complex (Fig. 45).[190] It shows a highly selective turn-on response towards S^{2-} over other common anion species in aqueous solution. The sequestration of complexed Cu^{2+} from **88** by S^{2-} is the origin for the turn-on response. The S^{2-}-induced removal of Cu^{2+} from **88** allows this probe to be able to detect 10 μM H_2S in an aqueous solution at pH 7.4, but it shows a fluorescence enhancement upon addition of 10 mM GSH. In order to improve the H_2S sensing selectivity over biological thiols, inorganic sulfur compounds, ROS and RNS species, Nagano and co-workers have developed a new probe **89**, which is derived from an azamacrocyclic Cu^{2+} complex.[191] Considering the strong binding affinity of the azamacrocyclic ring for Cu^{2+}, it was expected that only H_2S would remove Cu^{2+} from the azamacrocyclic ring. In fact, **89** displays a highly sensitive "turn-on" response towards H_2S in HEPES buffer, and the fluorescence enhancement factor is about 50-fold. The H_2S sensing ability of **89** has been demonstrated upon pseudo enzymatic H_2S release in a cuvette and in real-time fluorescence imaging of intracellular H_2S in living cells. Probe **90** is also a Cu^{2+} complex formed by a 8-hydroxyquinoline-appended fluorescein derivative. It also displays a highly selective "turn-on" response towards S^{2-}.[192] By incorporating an 8-aminoquinoline ligand in an NIR fluorophore, Lin and co-workers reported a new NIR fluorescent probe (**91**) for S^{2-} in HEPES buffer.[193] The free ligand exhibits an NIR emission peak at 794 nm with a quantum yield of 0.11, and its Cu^{2+} complex (**91**) displays a very weak emission due to the quenching effect. This Cu^{2+} complex displays a 27-fold fluorescence enhancement upon S^{2-} addition. Its detection limit for S^{2-} was calculated to be 280 nM.

5.4 Phosphorescent probes for biothiols

Thiol molecules are abundant in living systems and play essential roles in the process of reversible redox reactions, and cellular detoxification and metabolism.[194–196] Developing suitable luminescent probes for the imaging of biothiols is of importance to clarify their exact functions. Of course, almost all the approaches for H_2S probes can be utilized to construct biothiol probes. Here we just show the phosphorescent probes for biothiol to display the application of phosphorescent metal complexes.

Ruthenium complex **92** was developed as a "turn-on" red-emitting phosphorescent probe for thiol by Ji and co-workers (Fig. 46).[197] Probe **92** is non-emissive due to the electron

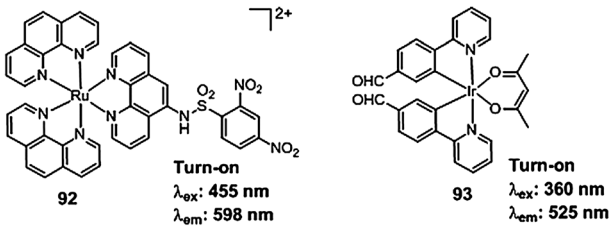

Fig. 46 Chemical structures of thiol probes **92** and **93**.

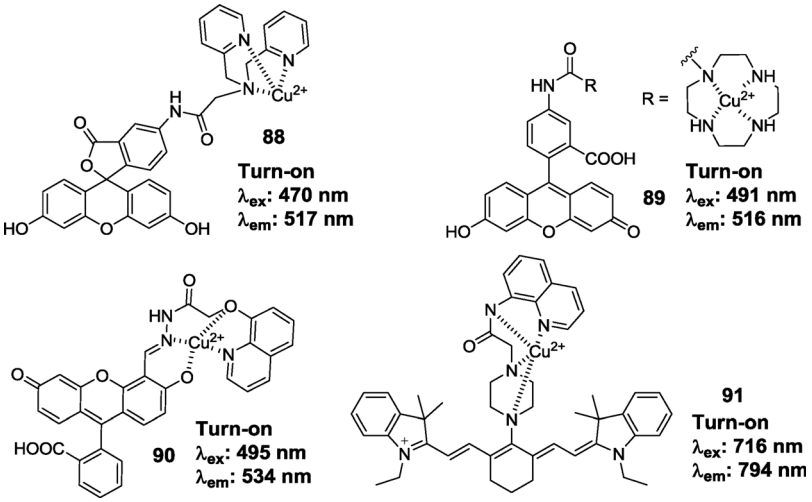

Fig. 45 Chemical structures of Cu^{2+} complex-based H_2S probes **88–91**.

transfer from Ru^{2+} to 2,4-dinitrobenzenesulfonyl (DNBS) inducing the corruption of MLCT. After the reaction with thiols such as L-cysteine, DNBS was cleaved from the 1,10-phenanthroline ligand and the MLCT process is re-established, displaying a turn-on fluorescent response (enhancement factor, ~90-fold). Utilizing the selective reaction of a carbaldehyde with cysteine/homocysteine (Hcy) to form thiazinane, a Hcy probe (**93**) based on an Ir^{3+} complex was developed (Fig. 46).[198] Upon the addition of Hcy, a new emission band centered at 525 nm in DMSO–HEPES buffer (50 mM, pH 7.2, 9:1, v:v) appeared, corresponding to a blue-shift of ~90 nm and a change in emission color from deep red to green can be observed by the naked eye.

5.5 Metal complex-based fluorescent probes for cyanide (CN^-)

5.5.1 Cu^{2+}/Zn^{2+} complex-based fluorescent probes for CN^-. Cyanide is extremely toxic to mammals, and can lead to vomiting, loss of consciousness, and finally death.[199] Fluorescent sensing of CN^- with a suitable probe is one of the most attractive methods for CN^- detection. For the construction of probes for CN^-, several strategies have been adopted including the coordination of CN^- to metal ion or boronic acid derivatives, hydrogen bonding with hydrogen donors, and CN^--induced specific reactions.[200,201] Since hydrogen bonding and CN^--related reactions can be affected by water, the related probes display normally low sensitivity and a slow response in aqueous media; coordination-based CN^- probes are more desirable for environmental and biological purposes.

Cu^{2+} complexes formed by fluorescent ligands are frequently utilized as turn-on CN^- probes, since these complexes display no fluorescence due to the emission quenching effect of paramagnetic Cu^{2+} and the fluorescence can be recovered distinctly by CN^--induced removal of the quenching effect. This approach is similar to that for probes of the sulfide anion. Since Cu^{2+} also shows high affinity to CN^-, Cu^{2+} removal from the non-fluorescent Cu^{2+} complexes by CN^- would recover the fluorescence. For example, by incorporating a BPA/Cu^{2+} system with IR-780, a water-soluble NIR fluorescent probe (**94**) for CN^- sensing was developed by Yoon and Park (Fig. 47).[202] This probe displays a NIR absorption and emission in HEPES buffer. It shows a highly selective turn-on response (14-fold) towards CN^- over other examined anion species. This probe has been applied to visualize CN^- anions produced by *P. aeruginosa* in *C. elegans*. In the case of a Cu^{2+} complex with high stability, CN^- addition will form a new CN^--containing complex rather than remove Cu^{2+}. The negatively charged CN^- coordination to Cu^{2+} would alter the electronic configuration of Cu^{2+} and disrupt the paramagnetic Cu^{2+}-induced quenching process, which results in fluorescence enhancement. For example, Guo and co-workers reported a new rhodamine–Cu^{2+} complex as a fluorescent probe (**95**) for CN^- (Fig. 47).[203] The vacant axial coordination sites for Cu^{2+} in **95** facilitate CN^- coordination to Cu^{2+}, and highly selective and sensitive turn-on (~10-fold) behavior for CN^- in aqueous solution can be observed. The binding stoichiometry is 2:2 and the detection limit for CN^- was estimated to be 0.14 μM.

Since Zn^{2+} does not quench emission and displays also a high affinity for CN^-, therefore, ratiometric probes for CN^- could be obtained when a coordination displacement approach was applied in a Zn^{2+} complex.[204] For example, Zn^{2+} coordination to **96** does not quench its fluorescence but results in a red-shift of emission from 480 to 530 nm in HEPES buffer. CN^- addition to a solution of the **96**/Zn^{2+} complex (**97**) leads to the recovery of the original emission maximum at 480 nm *via* Zn^{2+} removal. This ratiometric response of **97** towards CN^- is unique compared with other tested anion species.

5.5.2 Phosphorescent metal complex-based probes for CN^-. CN^- probes have also been constructed based on phosphorescent metal complexes. Two imidazole-based ruthenium complexes reported by Ye and co-workers show a selective turn-off response to CN^- in water (20 mM HEPES buffer, pH, 7.0) *via* formation of multiple hydrogen bonds with CN^-. The detection limits of **98** and **99** for CN^- in water are 100 and 5 μM,

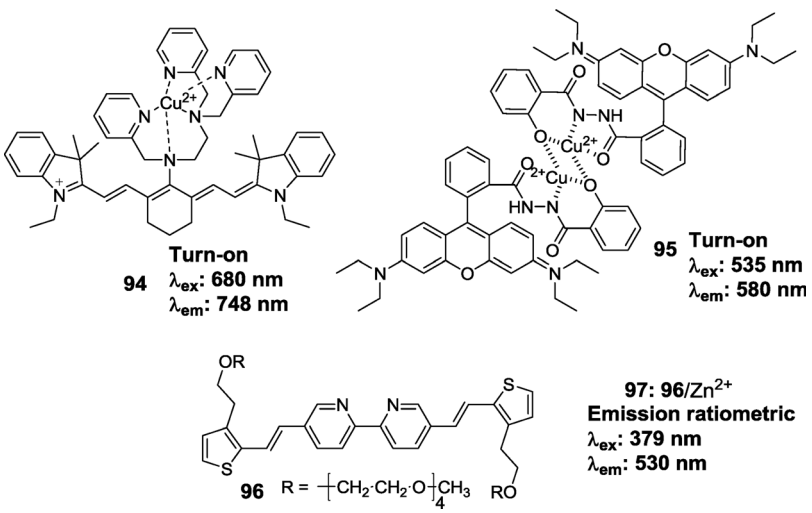

Fig. 47 Chemical structures of CN^- probes **94–97**.

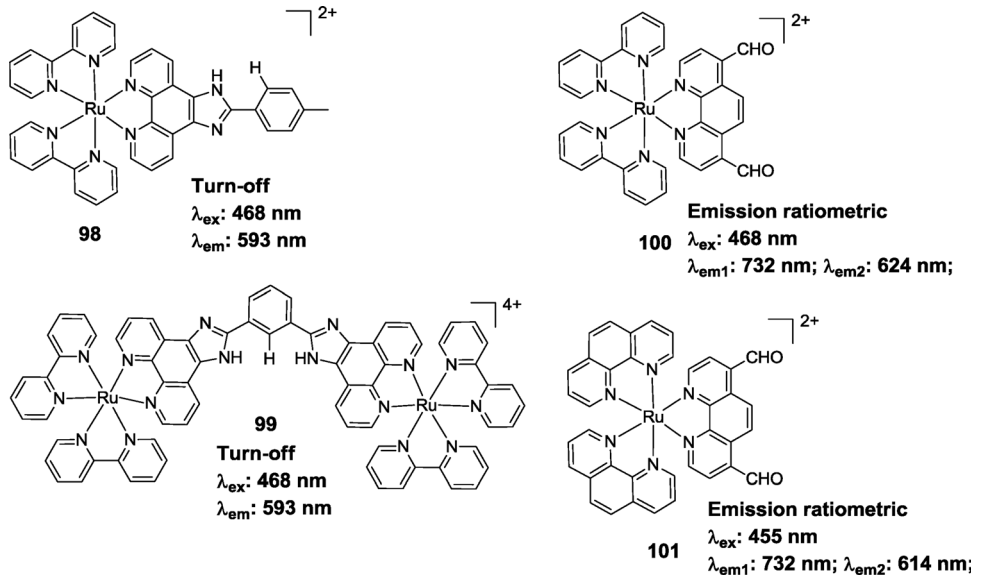

Fig. 48 Chemical structures of phosphorescent probes **98**–**101**.

respectively (Fig. 48). Probe **99** possesses a C-shaped cavity structure with a three-point hydrogen bonding set for CN^-, consisting of two N–H and one phenyl C–H sites. The hydrogen bonding of probes **98** and **99** with CN^- will induce a change in emission lifetime, which also can be exploited for CN^- detection.[205] Schmittel and co-workers reported two bis-heteroleptic ruthenium complexes **100** and **101** for CN^- detection by integrating carbaldehyde groups with a 1,10-phenanthroline ligand (Fig. 48).[206] Nucleophilic addition of CN^- to carbaldehyde to form cyanohydrin will be finished within 15 s in the presence of 2 equiv. CN^- in CH_3CN solution, which induces an emission enhancement of ~55-fold accompanied by an emission blue-shift of >100 nm. A high selectivity toward CN^- over other tested anions was observed for both probes. The reaction constants for CN^- for **100** and **101** were calculated to be $K_1 = 3.6 \pm 2.5 \times 10^8\ M^{-1}$ and $K_2 = 6.3 \pm 1.0 \times 10^6\ M^{-1}$ for **100** and $K_1 = 1.4 \pm 1.2 \times 10^9\ M^{-1}$ and $K_2 = 1.7 \pm 0.3 \times 10^7\ M^{-1}$ for **101**. Moreover, the CN^- addition induces a color change from orange-red to yellow, providing a simple real-time detection method for CN^-.

6. Concluding remarks and future perspectives

Coordination chemistry has made major impacts on the development of many different areas of chemistry in the past 100 years. It is also true for the fast growing field of molecular probes based on metal complexes or for the detection of metal cations. As we have seen from the examples discussed above, metal coordination plays a key role in the construction of fluorescent probes. Metal coordination effects on fluorescence of organic dyes and emissive metal complexes can be tuned or manipulated to fit the sensing scope. Here we list some of the challenges that may demand more advanced strategies in the future for the design and application of the probes.

Fundamental understanding of the metal coordination effect is not yet satisfactory. Rationales based on PeT, ICT, FRET and ESIPT processes are frequently applied in probe design, but they do not always work as expected. For example, metal coordination to the donor or acceptor group of ICT fluorophores should result in a shift of the emission/excitation band, but a number of ICT probes display only a ''turn-on'' or ''turn-off'' response to metal ions without any shift of emission/excitation band. On the other hand, paramagnetic metal cations such as Cu^{2+} and Fe^{3+} are generally considered to induce the emission quenching of fluorophores, however, some turn-on fluorescent probes for these cations were reported.[117] Electronic decoupling combined with rigid probe architecture or even the second coordination sphere were proposed to play roles in the effect, nevertheless, the exact origin for this phenomenon is not completely clear.

There is a huge scope in the exploration of probes based on emissive d-block transition metal complexes. Compared to the large body of probes based on organic dyes, successful examples of emissive metal complexes are rather limited. It may require fine tuning of ligands and structures to manipulate the complicated excited states of these complexes. Similarly, development of emissive Ln^{3+}-based biological probes with high quantum yields is also challenging due to their sensitivity to O_2 in aqueous solutions. On the other hand, the long-lived emission of Ln^{3+}- and d-block transition metal complexes can eliminate the interference of the fluorescence emitted by organic molecules within living samples, which provide formidable potential in time-resolved luminescence technology and time correlated single photon counting (TCSPC) techniques, and fluorescence lifetime imaging (FLIM).

Fluorescent probes for *in vivo* imaging are highly demanded, therefore complexes with NIR, two-photon excitability and aqueous solubility may be favorable and attractive. Multimodal probes combining fluorescence with other imaging methods

such as magnetic resonance imaging (MRI), single-photon emission computed tomography (SPECT) or positron emission tomography (PET) imaging have a very bright future for *in vivo* and clinical imaging. It is anticipated that metal coordination may play essential roles in designing multimodal imaging.

Taken together, coordination chemistry will continue to contribute to the further development of photoluminescent probes, as it has done in the past decades. Metal coordination offers effective means for modulating the fluorescent behaviors of the probe molecules.

Acknowledgements

We thank the National Basic Research Program of China (No. 2011CB935800) and National Natural Science Foundation of China (No. 10979019, 21131003, 91213305, 21271100, and 21021062) for financial support. Z.L. is thankful for support from the Natural Science Foundation of Shandong Province (No. ZR2011BQ010).

References

1 J. R. Lakowicz, *Principles of Fluorescence Spectroscopy*, Kluwer/Plenum, New York, 2nd edn, 1999.
2 *Fluorescent Chemoprobes for Ion and Molecule Recognition*, ed. A. W. Czarnik, American Chemical Society, Washington, D.C., 1993.
3 B. Valeur, *Molecular Fluorescence: Principles and Applications*, Wiley-VCH, Weinheim, 2001.
4 H. Kobayashi, M. Ogawa, R. Alford, P. L. Choyke and Y. Urano, *Chem. Rev.*, 2010, **110**, 2620.
5 R. Y. Tsien, *Annu. Rev. Biochem.*, 1998, **67**, 509.
6 T. Terai and T. Nagano, *Curr. Opin. Chem. Biol.*, 2008, **12**, 515.
7 M. Vendrell, D. Zhai, J. C. Er and Y.-T. Chang, *Chem. Rev.*, 2012, **112**, 4391.
8 M. E. Moragues, R. Martínez-Máñez and F. Sancenón, *Chem. Soc. Rev.*, 2011, **40**, 2593.
9 D. T. Quang and J. S. Kim, *Chem. Rev.*, 2010, **110**, 6280.
10 H. N. Kim, Z. Guo, W. Zhu, J. Yoon and H. Tian, *Chem. Soc. Rev.*, 2011, **40**, 79.
11 X. Chen, Y. Zhou, X. Peng and J. Yoon, *Chem. Soc. Rev.*, 2010, **39**, 2120.
12 Y. Zhou, Z. Xu and J. Yoon, *Chem. Soc. Rev.*, 2011, **40**, 2222.
13 E. M. Nolan and S. J. Lippard, *Chem. Rev.*, 2008, **108**, 3443.
14 A. T. Wright and E. V. Anslyn, *Chem. Soc. Rev.*, 2006, **35**, 14.
15 P. J. Jiang and Z. J. Guo, *Coord. Chem. Rev.*, 2004, **248**, 205.
16 A. P. de Silva, H. Q. N. Gunaratne, T. Gunnlaugsson, A. J. M. Huxley, C. P. McCoy, J. T. Rademacher and T. E. Rice, *Chem. Rev.*, 1997, **97**, 1515.
17 Q. Zhao, F. Li and C. Huang, *Chem. Soc. Rev.*, 2011, **40**, 2508.
18 Y. Yang, Q. Zhao, W. Feng and F. Li, *Chem. Rev.*, DOI: 10.1021/cr2004103.
19 D. Parker, *Coord. Chem. Rev.*, 2000, **205**, 109.
20 T. Gunnlaugsson, M. Glynn, G. M. Tocci, P. E. Kruger and F. M. Pfeffer, *Coord. Chem. Rev.*, 2006, **250**, 3094.
21 S. Shinoda and H. Tsukube, *Analyst*, 2011, **136**, 431.
22 Q. Zhao, F. Li and C. Huang, *Chem. Soc. Rev.*, 2010, **39**, 3007.
23 A. Thibon and V. C. Pierre, *Anal. Bioanal. Chem.*, 2009, **394**, 107.
24 B. Valeur and I. Leray, *Coord. Chem. Rev.*, 2000, **205**, 3.
25 A. P. de Silva, T. S. Moody and G. D. Wright, *Analyst*, 2009, **134**, 2385.
26 H. J. Carlson and R. E. Campbell, *Curr. Opin. Biotechnol.*, 2009, **20**, 19.
27 J. S. Kim and D. T. Quang, *Chem. Rev.*, 2007, **107**, 3780.
28 C. Lodeiro and F. Pina, *Coord. Chem. Rev.*, 2009, **253**, 1353.
29 J. Wu, W. Liu, J. Ge, H. Zhang and P. Wang, *Chem. Soc. Rev.*, 2011, **40**, 3483.
30 K. Kiyose, S. Aizawa, E. Sasaki, H. Kojima, K. Hanaoka, T. Terai, Y. Urano and T. Nagano, *Chem.–Eur. J.*, 2009, **15**, 9191.
31 M. Kasha, *J. Chem. Phys.*, 1952, **20**, 71.
32 M. A. El-Sayed, *Acc. Chem. Res.*, 1968, **1**, 8.
33 P. Svejda, A. H. Maki and R. R. Anderson, *J. Am. Chem. Soc.*, 1978, **100**, 7138.
34 H. Masuhara, H. Shioyama, T. Saito, K. Hamada, S. Yasoshima and N. Mataga, *J. Phys. Chem.*, 1984, **88**, 5868.
35 C. N. Burress, M. I. Bodine, O. Elbjeirami, J. H. Reibenspies, M. A. Omary and F. P. Gabbai, *Inorg. Chem.*, 2007, **46**, 1388.
36 H. N. Kim, W. X. Ren, J. S. Kim and J. Yoon, *Chem. Soc. Rev.*, 2012, **41**, 3210.
37 Z. R. Grabowski and K. Rotkiewicz, *Chem. Rev.*, 2003, **103**, 3899.
38 S. Sumalekshmy, M. M. Henary, N. Siegel, P. V. Lawson, Y. Wu, K. Schmidt, J.-L. Brédas, J. W. Perry and C. J. Fahrni, *J. Am. Chem. Soc.*, 2007, **129**, 11888.
39 P. Carol, S. Sreejith and A. Ajayaghosh, *Chem.–Asian J.*, 2007, **2**, 338.
40 W. Jiang, Q. Fu, H. Fan and W. Wang, *Chem. Commun.*, 2008, 259.
41 F. Qian, C. Zhang, Y. Zhang, W. He, X. Gao, P. Hu and Z. Guo, *J. Am. Chem. Soc.*, 2009, **131**, 1460.
42 N. C. Lim and C. Brückner, *Chem. Commun.*, 2004, 1094.
43 K. E. Sapsford, L. Berti and I. L. Medintz, *Angew. Chem., Int. Ed.*, 2006, **45**, 4562.
44 Z. Zhou, M. Yu, H. Yang, K. Huang, F. Li, T. Yi and C. Huang, *Chem. Commun.*, 2008, 3387.
45 K. Sreenath, J. R. Allen, M. W. Davidson and L. Zhu, *Chem. Commun.*, 2011, **47**, 11730.
46 J. L. Vinkenborg, T. J. Nicolson, E. A. Bellomo, M. S. Koay, G. A. Rutter and M. Merkx, *Nat. Methods*, 2009, **6**, 737.
47 (*a*) J. G. Park, Y. Qin, D. F. Galati and A. E. Palmer, *ACS Chem. Biol.*, 2012, **7**, 1636; (*b*) P. J. Dittmer, J. G. Miranda, J. A. Gorski and A. E. Palmer, *J. Biol. Chem.*, 2009, **284**, 16289.
48 S. V. Wegner, H. Arslan, M. Sunbul, J. Yin and C. He, *J. Am. Chem. Soc.*, 2010, **132**, 2567.
49 H. S. Jung, M. Park, D. Y. Han, E. Kim, C. Lee, S. Ham and J. S. Kim, *Org. Lett.*, 2009, **11**, 3378.

50 H. J. Kim, J. Hong, A. Hong, S. Ham, J. H. Lee and J. S. Kim, *Org. Lett.*, 2008, **10**, 1963.
51 M. M. Henary, Y. Wu and C. J. Fahrni, *Chem.–Eur. J.*, 2004, **10**, 3015.
52 M. M. Henary and C. J. Fahrni, *J. Phys. Chem. A*, 2002, **106**, 5210.
53 J. E. Kwon, S. Lee, Y. You, K.-H. Baek, K. Ohkubo, J. Cho, S. Fukuzumi, I. Shin, S. Y. Park and W. Nam, *Inorg. Chem.*, 2012, **51**, 8760.
54 M. E. Jun, B. Roy and K. H. Ahn, *Chem. Commun.*, 2011, **47**, 7583.
55 V. Dujols, F. Ford and A. W. Czarnik, *J. Am. Chem. Soc.*, 1997, **119**, 7386.
56 X. Chen, T. Pradhan, F. Wang, J. S. Kim and J. Yoon, *Chem. Rev.*, 2012, **112**, 1910.
57 C. P. Montgomery, B. S. Murray, E. J. New, R. Pal and D. Parker, *Acc. Chem. Res.*, 2009, **42**, 925.
58 V. W.-W. Yam and K. M.-C. Wong, *Chem. Commun.*, 2011, **47**, 11579.
59 N. Sabbatini, M. Guardigli and J.-M. Lehn, *Coord. Chem. Rev.*, 1993, **123**, 201.
60 S. U. Pandya, J. Yu and D. Parker, *Dalton Trans.*, 2006, 2757.
61 J. Yuan and G. Wang, *TrAC, Trends Anal. Chem.*, 2006, **25**, 490.
62 K. Hanaoka, K. Kikuchi, H. Kojima, Y. Urano and T. Nagano, *J. Am. Chem. Soc.*, 2004, **126**, 12470.
63 A. Thibon and V. C. Pierre, *J. Am. Chem. Soc.*, 2009, **131**, 434.
64 Y. Bretonniere, M. J. Cann, D. Parker and R. Slater, *Chem. Commun.*, 2002, 1930.
65 Y. Bretonniere, M. J. Cann, D. Parker and R. Slater, *Org. Biomol. Chem.*, 2004, **2**, 1624.
66 J. P. Leonard, C. M. G. dos Santos, S. E. Plush, T. McCabe and T. Gunnlaugsson, *Chem. Commun.*, 2007, 129, 274.
67 Q. Zhao, F. Li and C. Huang, *Chem. Soc. Rev.*, 2011, **40**, 2508.
68 Y. Chi and P. T. Chou, *Chem. Soc. Rev.*, 2010, **39**, 638.
69 W. Lu, W.-M. Kwok, C. Ma, C. T.-L. Chan, M.-X. Zhu and C.-M. Che, *J. Am. Chem. Soc.*, 2011, **133**, 14120.
70 K. R. J. Thomas, M. Velusamy, J. T. Lin, C. H. Chien, Y. T. Tao, Y. S. Wen, Y. H. Hu and P. T. Chou, *Inorg. Chem.*, 2005, **44**, 5677.
71 Y. You and W. Nam, *Chem. Soc. Rev.*, 2012, **41**, 7061.
72 W. Lu, B. X. Mi, M. C. W. Chan, Z. Hui, C. M. Che, N. Zhu and S. T. Lee, *J. Am. Chem. Soc.*, 2004, **126**, 4958.
73 M. S. Lowry and S. Bernhard, *Chem.–Eur. J.*, 2006, **12**, 7970.
74 Y. You, S. Lee, T. Kim, K. Ohkubo, W.-S. Chae, S. Fukuzumi, G.-J. Jhon, W. Nam and S. J. Lippard, *J. Am. Chem. Soc.*, 2011, **133**, 18328.
75 P. K. M. Siu, S. W. Lai, W. Lu, N. Zhu and C. M. Che, *Eur. J. Inorg. Chem.*, 2003, 2749.
76 M. W. Louie, H. W. Liu, M. H. C. Lam, T. C. Lau and K. K. W. Lo, *Organometallics*, 2009, **28**, 4297.
77 S. Lamansky, P. Djurovich, D. Murphy, F. Abdel-Razzaq, H. E. Lee, C. Adachi, P. E. Burrows, S. R. Forrest and M. E. Thompson, *J. Am. Chem. Soc.*, 2001, **123**, 4304.
78 Y. You and S. Y. Park, *J. Am. Chem. Soc.*, 2005, **127**, 12438.
79 M. Polson, M. Ravaglia, S. Fracasso, M. Garavelli and F. Scandola, *Inorg. Chem.*, 2005, **44**, 1282.
80 C. K. Li, X. X. Lu, K. M. C. Wong, C. L. Chan, N. Zhu and V. W. W. Yam, *Inorg. Chem.*, 2004, **43**, 7421.
81 S. Lamansky, P. Djurovich, D. Murphy, F. Abdel-Razzaq, R. Kwong, I. Tsyba, M. Bortz, B. Mui, R. Bau and M. E. Thompson, *Inorg. Chem.*, 2001, **40**, 1704.
82 S. W. Lai, M. C. W. Chan, T. C. Cheung, S. M. Peng and C. M. Che, *Inorg. Chem.*, 1999, **38**, 4046.
83 C. K. Li, X. X. Lu, K. M. C. Wong, C. L. Chan, N. Zhu and V. W. W. Yam, *Inorg. Chem.*, 2004, **43**, 7421.
84 Q. Zhao, L. Li, F. Y. Li, M. X. Yu, Z. P. Liu, T. Yi and C. H. Huang, *Chem. Commun.*, 2008, 685.
85 K. W. Huang, H. Z. Wu, M. Shi, F. Y. Li, T. Yi and C. H. Huang, *Chem. Commun.*, 2009, 1243.
86 Y. You and S. Y. Park, *Adv. Mater.*, 2008, **20**, 3820.
87 Y. Fan, Y. M. Zhu, F. R. Dai, L. Y. Zhang and Z. N. Chen, *Dalton Trans.*, 2007, 3885.
88 Y. Sun and S. Wang, *Inorg. Chem.*, 2009, **48**, 3755.
89 Q. Zhao, T. Y. Cao, F. Y. Li, X. H. Li, H. Jing, T. Yi and C. H. Huang, *Organometallics*, 2007, **26**, 2077.
90 R. Zhang, Z. Ye, Y. Yin, G. Wang, D. Jin, J. Yuan and J. A. Piper, *Bioconjugate Chem.*, 2012, **23**, 725.
91 L.-Q. Song, J. Feng, X.-S. Wang, J.-H. Yu, Y.-J. Hou, P.-H. Xie, B.-W. Zhang, J.-F. Xiang, X.-C. Ai and J.-P. Zhang, *Inorg. Chem.*, 2003, **42**, 3393.
92 B. R. Spencer, B. J. Kraft, C. G. Hughes, M. Pink and J. M. Zaleski, *Inorg. Chem.*, 2010, **49**, 11333.
93 E. C. Glazer, D. Magde and Y. Tor, *J. Am. Chem. Soc.*, 2007, **129**, 8544.
94 E. C. Glazer, D. Magde and Y. Tor, *J. Am. Chem. Soc.*, 2005, **127**, 4190.
95 A. El Nahhas, C. Consani, A. M. Blanco-Rodríguez, K. M. Lancaster, O. Braem, A. Cannizzo, M. Towrie, I. P. Clark, S. Záliš, M. Chergui and A. Vlček, Jr., *Inorg. Chem.*, 2011, **50**, 2932.
96 L. Wallace, C. Woods and D. P. Rillema, *Inorg. Chem.*, 1995, **34**, 2875.
97 Y. You, J. Seo, S. H. Kim, K. S. Kim, T. K. Ahn, D. Kim and S. Y. Park, *Inorg. Chem.*, 2008, **47**, 1476.
98 Y. You and S. Y. Park, *J. Am. Chem. Soc.*, 2005, **127**, 12438.
99 W. L. Jolly, *Modern Inorganic Chemistry*, McGraw-Hill, New York, 1984, ISBN 0-07-032760-2.
100 H. M. N. H. Irving and R. J. P. Williams, *J. Chem. Soc.*, 1953, 3192.
101 Z. Liu, C. Zhang, Y. Li, Z. Wu, F. Qian, X. Yang, W. He, X. Gao and Z. Guo, *Org. Lett.*, 2009, **11**, 795.
102 D. K. Cabinness and D. W. Margerum, *J. Am. Chem. Soc.*, 1969, **91**, 6540.
103 F. A. Cotton and G. Wilkinson, *Advanced Inorganic Chemistry*, Wiley, 5th edn, 1988.
104 K. J. Barnham, C. L. Masters and A. I. Bush, *Nat. Rev. Drug Discovery*, 2004, **3**, 205.
105 E. Gaggelli, H. Kozlowski, D. Valensin and G. Valensin, *Chem. Rev.*, 2006, **106**, 1995.

106 D. Brown and H. Kozlowski, *Dalton Trans.*, 2004, 1907.
107 G. Millhauser, *Acc. Chem. Res.*, 2004, **37**, 79.
108 J. Valentine and P. J. Hart, *Proc. Natl. Acad. Sci. U. S. A.*, 2003, **100**, 3617.
109 S. Lutsenko, A. Gupta, J. L. Burkhead and V. Zuzel, *Arch. Biochem. Biophys.*, 2008, **476**, 22.
110 I. Bertini and A. Rosato, *Cell. Mol. Life Sci.*, 2008, **65**, 89.
111 S. G. Kaler, *Nat. Rev. Neurosci.*, 2011, **7**, 15.
112 A. I. Bush, *Curr.Opin. Chem. Biol.*, 2000, **4**, 184.
113 M. P. Cuajungco and G. J. Lees, *Neurobiol. Dis.*, 1997, **4**, 137.
114 B. P. Espósito, S. Epsztejn, W. Breuer and Z. I. Cabantchik, *Anal. Biochem.*, 2002, **304**, 1.
115 J. Burgess and M. V. Twigg, *Iron: Inorganic & Coordination Chemistry. Encyclopedia of Inorganic Chemistry*, 2006.
116 Z. Yang, C. Yan, Y. Chen, C. Zhu, C. Zhang, X. Dong, W. Yang, Z. Guo, Y. Lu and W. He, *Dalton Trans.*, 2011, **40**, 2173.
117 J. L. Bricks, A. Kovalchuk, C. Trieflinger, M. Nofz, M. Büschel, A. I. Tolmachev, J. Daub and K. Rurack, *J. Am. Chem. Soc.*, 2005, **127**, 13522.
118 Z. Yang, M. She, B. Yin, J. Cui, Y. Zhang, W. Sun, J. Li and Z. Shi, *J. Org. Chem.*, 2012, **77**, 1143.
119 W. Lin, L. Long, L. Yuan, Z. Cao and J. Feng, *Anal. Chim. Acta*, 2009, **634**, 262.
120 M. Xu, S. Wu, F. Zeng and C. Yu, *Langmuir*, 2010, **26**, 4529.
121 P. Li, L. Fang, H. Zhou, W. Zhang, X. Wang, N. Li, H. Zhong and B. Tang, *Chem.–Eur. J.*, 2011, **17**, 10520.
122 S. C. Burdette and S. J. Lippard, *Proc. Natl. Acad. Sci. U. S. A.*, 2003, **100**, 3605.
123 K. Kikuchi, H. Komatsu and T. Nagano, *Curr. Opin. Chem. Biol.*, 2004, **8**, 182.
124 E. L. Que, D. W. Domaille and C. J. Chang, *Chem. Rev.*, 2008, **108**, 1517.
125 Z. Xu, J. Yoon and D. R. Spring, *Chem. Soc. Rev.*, 2010, **39**, 1996.
126 E. Tomat and S. J. Lippard, *Curr. Opin. Chem. Biol.*, 2010, **14**, 225.
127 E. M. Nolan and S. J. Lippard, *Acc. Chem. Res.*, 2009, **42**, 193.
128 M. P. Murphy and R. A. Smith, *Annu. Rev. Pharmacol. Toxicol.*, 2007, **47**, 629.
129 G. Masanta, C. S. Lim, H. J. Kim, J. H. Han, H. M. Kim and B. R. Cho, *J. Am. Chem. Soc.*, 2011, **133**, 5698.
130 Z. Liu, C. Zhang, Y. Chen, W. He and Z. Guo, *Chem. Commun.*, 2012, **48**, 8365.
131 L. Xue, G. Li, C. Yu and H. Jiang, *Chem.–Eur. J.*, 2011, **18**, 1050.
132 Y. Qin, P. J. Dittmer, J. G. Park, K. B. Jansen and A. E. Palmer, *Proc. Natl. Acad. Sci. U. S. A.*, 2011, **108**, 7351.
133 K. Hanaoka, K. Kikuchi, S. Kobayashi and T. Nagano, *J. Am. Chem. Soc.*, 2007, **129**, 13502.
134 J. C. Araya, J. Gajardo, S. A. Moya, P. Aguirre, L. Toupet, J. A. G. Williams, M. Escadeillas, H. L. Bozec and V. Guerchais, *New J. Chem.*, 2010, **34**, 21.
135 P.-K. Lee, W. H.-T. Law, H.-W. Liu and K. K.-W. Lo, *Inorg. Chem.*, 2011, **50**, 8570.
136 V. A. Rapisarda, S. I. Volentini, R. N. Farias and E. M. Massa, *Anal. Biochem.*, 2002, **307**, 105.
137 L. Yang, R. McRae, M. M. Henary, R. Patel, B. Lai, S. Vogt and C. J. Fahrni, *Proc. Natl. Acad. Sci. U. S. A.*, 2005, **102**, 11179.
138 L. Zeng, E. W. Miller, A. Pralle, E. Y. Isacoff and C. J. Chang, *J. Am. Chem. Soc.*, 2006, **128**, 10.
139 S. C. Dodani, S. C. Leary, P. A. Cobine, D. R. Winge and C. J. Chang, *J. Am. Chem. Soc.*, 2011, **133**, 8606.
140 T. Hirayama, G. C. Van de Bittner, L. W. Gray, S. Lutsenko and C. J. Chang, *Proc. Natl. Acad. Sci. U. S. A.*, 2012, **109**, 2228.
141 E. Ballesteros, D. Moreno, T. Gómez, T. Rodríguez, J. Rojo, M. García-Valverde and T. Torroba, *Org. Lett.*, 2009, **11**, 1269.
142 D. W. Domaille, L. Zeng and C. J. Chang, *J. Am. Chem. Soc.*, 2010, **132**, 1194.
143 Z. Xu, Y. Xiao, X. Qian, J. Cui and D. Cui, *Org. Lett.*, 2005, **7**, 889.
144 Z. Xu, J. Pan, D. R. Spring, J. Cui and J. Yoon, *Tetrahedron*, 2010, **66**, 1678.
145 Z. Xu, X. Qian and J. Cui, *Org. Lett.*, 2005, **7**, 3029.
146 H. S. Jung, M. Park, D. Y. Han, E. Kim, C. Lee, S. Ham and J. S. Kim, *Org. Lett.*, 2009, **11**, 3378.
147 Z. Xu, J. Yoon and D. R. Spring, *Chem. Commun.*, 2010, **46**, 2563.
148 R. F. H. Viguier and A. N. Hulme, *J. Am. Chem. Soc.*, 2006, **128**, 11370.
149 Y. You, Y. Han, Y.-M. Lee, S. Y. Park, W. Nam and S. J. Lippard, *J. Am. Chem. Soc.*, 2011, **133**, 11488.
150 Z. Xie, K. Wang, C. Zhang, Z. Yang, Y. Chen, Z. Guo, G.-Y. Lu and W. He, *New J. Chem.*, 2011, **35**, 607.
151 W. Ma, Q. Xu, J. Du, B. Song, X. Peng, Z. Wang, G. Li and X. Wang, *Spectrochim. Acta, Part A*, 2010, **76**, 248.
152 Q. Zou, L. Zou and H. Tian, *J. Mater. Chem.*, 2011, **21**, 14441.
153 Q. Zou and H. Tian, *Sens. Actuators, B*, 2010, **149**, 20.
154 Y. Chen, C. Zhu, Z. Yang, J. Li, Y. Jiao, W. He, J. Chen and Z. Guo, *Chem. Commun.*, 2012, **48**, 5094.
155 C. S. Lim, D. W. Kang, Y. S. Tian, J. H. Han, H. L. Hwang and B. R. Cho, *Chem. Commun.*, 2010, **46**, 2388.
156 Z. Xie, K. Wang, C. Zhang, Z. Yang, Y. Chen, Z. Guo, G.-Y. Lu and W. He, *New J. Chem.*, 2011, **35**, 607.
157 M. H. Lee, S. W. Lee, S. H. Kim, C. Kang and J. S. Kim, *Org. Lett.*, 2009, **11**, 2101.
158 B. P. Joshi, C. R. Lohani and K.-H. Lee, *Org. Biomol. Chem.*, 2010, **8**, 3220.
159 Y. Zhou, C.-Y. Zhu, X.-S. Gao, X.-Y. You and C. Yao, *Org. Lett.*, 2010, **12**, 2566.
160 Y. Liu, X. Dong, J. Sun, C. Zhong, B. Li, X. You, B. Liu and Z. Liu, *Analyst*, 2012, **137**, 1837.
161 M. Taki, M. Desaki, A. Ojida, S. Iyoshi, T. Hirayama, I. Hamachi and Y. Yamamoto, *J. Am. Chem. Soc.*, 2008, **130**, 12564.
162 Z. Liu, C. Zhang, W. He, Z. Yang, X. Gao and Z. Guo, *Chem. Commun.*, 2010, **46**, 6138.

163 C. Park and J.-I. Hong, *Tetrahedron Lett.*, 2010, **51**, 1960.
164 Y. J. Jang, E. J. Jun, Y. J. Lee, Y. S. Kim, J. S. Kim and J. Yoon, *J. Org. Chem.*, 2005, **70**, 9603.
165 D. H. Lee, J. H. Im, S. U. Son, Y. K. Chung and J.-I. Hong, *J. Am. Chem. Soc.*, 2003, **125**, 7752.
166 D. H. Lee, S. Y. Kim and J.-I. Hong, *Angew. Chem., Int. Ed.*, 2004, **43**, 4777.
167 G. Su, Z. Liu, Z. Xie, F. Qian, W. He and Z. Guo, *Dalton Trans.*, 2009, 7888.
168 J. F. Zhang, M. Park, W. X. Ren, Y. Kim, S. J. Kim, J. H. Jung and J. S. Kim, *Chem. Commun.*, 2011, **47**, 3568.
169 A. Nonaka, S. Horie, T. D. James and Y. Kubo, *Org. Biomol. Chem.*, 2008, **6**, 3621.
170 H. K. Cho, D. H. Lee and J.-I. Hong, *Chem. Commun.*, 2005, 1690.
171 H. N. Lee, Z. Xu, S. K. Kim, K. M. K. Swamy, Y. Kim, S.-J. Kim and J. Yoon, *J. Am. Chem. Soc.*, 2007, **129**, 3828.
172 J. Wen, Z. Geng, Y. Yin, Z. Zhang and Z. Wang, *Dalton Trans.*, 2011, **40**, 1984.
173 W.-H. Chen, Y. Xing and Y. Pang, *Org. Lett.*, 2011, **13**, 1362.
174 A. Ojida, I. Takashima, T. Kohira, H. Nonaka and I. Hamachi, *J. Am. Chem. Soc.*, 2008, **130**, 12095.
175 A. S. Rao, D. Kim, H. Nam, H. Jo, K. H. Kim, C. Ban and K. H. Ahn, *Chem. Commun.*, 2012, **48**, 3206.
176 H. Wu, C. He, Z. Lin, Y. Liu and C. Duan, *Inorg. Chem.*, 2009, **48**, 408.
177 Y. Kurishita, T. Kohira, A. Ojida and I. Hamachi, *J. Am. Chem. Soc.*, 2010, **132**, 13290.
178 T. Nagano and T. Yoshimura, *Chem. Rev.*, 2002, **102**, 1235.
179 S. A. Hilderbrand, M. H. Lim and S. J. Lippard, in *Topics in Fluorescence Spectroscopy*, ed. C. D. Geddes and J. R. Lakowicz, Springer, Berlin, 2005, p. 163.
180 K. J. Franz, N. Singh and S. J. Lippard, *Angew. Chem., Int. Ed.*, 2000, **39**, 2120.
181 M. H. Lim and S. J. Lippard, *J. Am. Chem. Soc.*, 2005, **127**, 12170.
182 M. H. Lim, B. A. Wong, W. H. Pitcock, Jr., D. Mokshagundam, M.-H. Baik and S. J. Lippard, *J. Am. Chem. Soc.*, 2006, **128**, 14364.
183 M. E. Murphy and H. Sies, *Proc. Natl. Acad. Sci. U. S. A.*, 1991, **88**, 10860.
184 J. Rosenthal and S. J. Lippard, *J. Am. Chem. Soc.*, 2010, **132**, 5536.
185 Y. Zhou, K. Liu, J.-Y. Li, Y. Fang, T.-C. Zhao and C. Yao, *Org. Lett.*, 2011, **13**, 1290.
186 H. Kimura, Y. Nagai, K. Umemura and Y. Kimura, *Antioxid. Redox Signaling*, 2005, **7**, 795.
187 L. Li, P. Rose and P. K. Moore, *Annu. Rev. Pharmacol. Toxicol.*, 2011, **51**, 169.
188 T. W. Miller, J. S. Isenberg and D. D. Roberts, *Chem. Rev.*, 2009, **109**, 3099.
189 R. d'Emmanuele di Villa Bianca, R. Sorrentino, V. Mirone and G. Cirino, *Nat. Rev. Urol.*, 2011, **8**, 286.
190 M. G. Choi, S. Cha, H. Lee, H. L. Jeon and S.-K. Chang, *Chem. Commun.*, 2009, 7390.
191 K. Sasakura, K. Hanaoka, N. Shibuya, Y. Mikami, Y. Kimura, T. Komatsu, T. Ueno, T. Terai, H. Kimura and T. Nagano, *J. Am. Chem. Soc.*, 2011, **133**, 18003.
192 F. Hou, L. Huang, P. Xi, J. Cheng, X. Zhao, G. Xie, Y. Shi, F. Cheng, X. Yao, D. Bai and Z. Zeng, *Inorg. Chem.*, 2012, **51**, 2454.
193 X. Cao, W. Lin and L. He, *Org. Lett.*, 2011, **13**, 4716.
194 J. B. Schulz, J. Lindenau, J. Seyfried and J. Dichgans, *Eur. J. Biochem.*, 2000, **267**, 4904.
195 S. Seshadri, A. Beiser, J. Selhub, P. F. Jacques, I. H. Rosenberg, R. B. D'Agostino, P. W. F. Wilson and P. A. Wolf, *N. Engl. J. Med.*, 2002, **346**, 476.
196 Z. A. Wood, E. Schröder, J. Robin Harris and L. B. Poole, *Trends Biochem. Sci.*, 2003, **28**, 32.
197 S. Ji, H. Guo, X. Yuan, X. Li, H. Ding, P. Gao, C. Zhao, W. Wu, W. Wu and J. Zhao, *Org. Lett.*, 2010, **12**, 2876.
198 H. L. Chen, Q. Zhao, Y. B. Wu, F. Y. Li, H. Yang, T. Yi and C. H. Huang, *Inorg. Chem.*, 2007, **46**, 11075.
199 K. W. Kulig, *Cyanide Toxicity*, U. S. Department of Health and Human Services, Atlanta, GA, 1991.
200 Z. Liu, X. Wang, Z. Yang and W. He, *J. Org. Chem.*, 2011, **76**, 10286.
201 Z. Xu, X. Chen, H. N. Kim and J. Yoon, *Chem. Soc. Rev.*, 2010, **39**, 127.
202 X. Chen, S.-W. Nam, G.-H. Kim, N. Song, Y. Jeong, I. Shin, S. K. Kim, J. Kim, S. Park and J. Yoon, *Chem. Commun.*, 2010, **46**, 8953.
203 Y. Liu, X. Lv, Y. Zhao, J. Liu, Y.-Q. Sun, P. Wang and W. Guo, *J. Mater. Chem.*, 2012, **22**, 1747.
204 K. P. Divya, S. Sreejith, B. Balakrishna, P. Jayamurthy, P. Aneesa and A. Ajayaghosh, *Chem. Commun.*, 2010, **46**, 6069.
205 H.-J. Mo, Y. Shen and B.-H. Ye, *Inorg. Chem.*, 2012, **51**, 7174.
206 S. Khatua, D. Samanta, J. W. Bats and M. Schmittel, *Inorg. Chem.*, 2012, **51**, 7075.

